Breaking the Kurtosis–Capacity Tradeoff in Random ISAC Signals via Short-Block Spherical and Clutter-Trench Constellation Shaping

Sai Thrinay Potta, *Member, IEEE*

***Abstract*—Under independent and identically distributed (i.i.d.) symbol signaling in integrated sensing and communications (ISAC), the normalized ranging and delay-Doppler sidelobe variance $(\kappa_{\mathrm{marg}}-1)/N$ is determined by the scalar amplitude kurtosis $\kappa_{\mathrm{marg}}=\mathbb{E}[|S|^4]/(\mathbb{E}[|S|^2])^2$. Constant-modulus phase-shift keying ($|S_{n,m}|=1$, $\kappa_{\mathrm{marg}}=1$) gives zero modulation sidelobes at $q=0$ with a $\frac{1}{2}\log_2(\pi e/2)=1.53$ dB high-SNR shaping gap to additive white Gaussian noise (AWGN) capacity $C_{\mathrm{AWGN}}(\rho)=\log_2(1+\rho)$; Gaussian and probabilistically shaped constellations ($\kappa_{\mathrm{marg}}\in(1.80,2]$) close the shaping gap with sidelobe variance $(\kappa_{\mathrm{marg}}-1)/N>0$. Coupling symbol intensities $r_{n,m}=|S_{n,m}|^2$ across short blocks within one 3GPP 5G/6G New Radio (NR) slot ($M=14$ orthogonal frequency-division multiplexing symbols, or $M=16$ dyadic symbols) decouples sidelobe variance from κ_{marg}. From the $N^2\times N^2$ fourth-order moment matrix $\mathbf{S}_{\mathrm{mom}}=\mathbf{I}_{N^2}+\mathbf{S}_1+\mathbf{S}_2+\mathbf{S}_{\mathrm{cov}}$ of non-i.i.d. proper circularly symmetric ensembles, the ambiguity variance reduces to a Rayleigh quotient $\mathbf{f}^H\mathbf{C}\mathbf{f}$ of the intensity covariance matrix $\mathbf{C}=\mathrm{Cov}(\mathbf{r})$. Full-frame 1D spherical shaping on $\sqrt{N}\,\mathbb{S}^{2N-1}$ incurs an $N/(N-1)$ simplex-exchangeability penalty; 2D slow-time spherical and subspace-simplex clutter-trench shaping place any d_{null}-dimensional low-Doppler clutter subspace $\mathcal{V}_{\mathrm{null}}$ into $\ker(\mathbf{C}_{\mathrm{slow}})$. By Parseval's identity, radial variance outside $\mathcal{Q}_{\mathrm{null}}$ scales by $M/(M-d_{\mathrm{null}})$ with $\kappa_{\mathrm{proj}}(M,d_{\mathrm{null}})=(2M+1-d_{\mathrm{null}})/(M+1)\to 2$, finite-$M$ rate loss $\Delta I_{\mathrm{sphere}}(L,\rho)=\frac{1}{L}D_{\mathrm{KL}}(f_{R^2_{\mathrm{sph}}}\|f_{R^2_{\mathrm{G}}})$, radial data-processing inequality (DPI) converse $\Delta I_{\mathrm{trench}}(M,d_{\mathrm{null}},\rho)\geq\Delta I_{\mathrm{sphere}}(M,\rho)$, and $R_{\mathrm{APSK}}(L)=4.0000$ b/s/Hz concentric $(4,8,16)$-APSK constant-composition distribution matching (CCDM) shells ($L\in\{7,8\}$). At $\rho=20$ dB, $d_{\mathrm{null}}=1$ gives $C_{\mathrm{AWGN}}-\Delta I_{\mathrm{sphere}}=6.5058$ b/s/Hz (97.7%, $M=14$) and 6.5249 b/s/Hz (98.0%, $M=16$) at $\mathrm{ISLR}_{\mathrm{self}}=2\sigma^2_{\mathrm{EVM}}=-35.49$ dB; $d_{\mathrm{null}}=3$ ($\mathcal{Q}_{\mathrm{null}}=\{0,\pm1\}$, 93.1% at $M=14$, $R_{\mathrm{APSK}}\in\{3.8125,3.8571\}$ b/s/Hz) gives $\mathrm{TCR}_{0.90}=-32.0$ dB ($+13.5$ dB over i.i.d. PAS-64QAM + MF; $+4.8$ dB over zero-forcing at $M=16$) and $\mathrm{CRLB}(\hat{\tau}_t)/\mathrm{CRLB}_{\mathrm{free}}(\hat{\tau}_t)=1.010$ (99.0% delay FIM; $+18.2$ dB target margin at $M=14$).**

***Index Terms*—Integrated sensing and communications (ISAC), ambiguity function, fourth-order kurtosis, spherical constellation shaping, constant-composition distribution matching (CCDM), cyclic-prefix OFDM, finite-blocklength information theory.**

I. Introduction

In sixth-generation (6G) integrated sensing and communications (ISAC) [1]–[3], [27], [28], a downlink multicarrier frame $\mathbf{S}\in\mathbb{C}^{N\times M}$ (N subcarriers, M slow-time symbols; $M=14$ in 3GPP TS 38.211 NR) carries random payload symbols $S_{n,m}\in\mathbb{C}$ rather than a fixed sequence $|S_{n,m}|=1$ [4]. Second-order statistics of the periodic autocorrelation function (P-ACF) $\tilde{r}_k$ and 2D delay-Doppler ambiguity function (AF) $\mathcal{A}_{\mathrm{FST}}(k,q)$ under random $S_{n,m}$ are given in [5]–[10]. For independent and identically distributed (i.i.d.) frequency-domain symbols $\{S_n\}_{n=0}^{N-1}$ with $\mathbb{E}[|S_n|^2]=1$ and proper circular phase symmetry, $\mathbb{E}[|\tilde{r}_k|^2]$ decomposes into a pulse-shaping mainlobe term and a modulation sidelobe floor [5]. Under i.i.d. QAM and PSK, cyclic-prefix orthogonal frequency-division multiplexing (CP-OFDM, $\mathbf{x}=\mathbf{F}_N^H\mathbf{s}$) achieves the minimum average ranging sidelobe variance over all unitary fast-time bases $\mathbf{U}\in\mathbb{C}^{N\times N}$ [6], with normalized 1D variance at lag $k\in\{1,\ldots,N-1\}$ equal to

$$\frac{1}{N}\mathbb{E}\Big[|\tilde{r}_k|^2\Big]=\kappa_{\mathrm{marg}}-1,\quad \kappa_{\mathrm{marg}}\triangleq\frac{\mathbb{E}[|S|^4]}{(\mathbb{E}[|S|^2])^2}. \tag{1}$$

In 2D discrete AF models over N subcarriers and M OFDM symbols [8], [10], correlating the raw time-domain waveform prior to per-subcarrier symbol derotation retains cross-subcarrier products $S_{n,m}S^*_{n',m}$ and a $1/N$ floor at $q\neq 0$ even under PSK. Pulse-Doppler OFDM radar receivers compute per-symbol range compression $\tilde{R}_{n,m}=S^*_{n,m}Y_{n,m}$ ($\tilde{r}_{k,m}=\sqrt{N}\,\mathbf{f}_{N,k}^H\mathbf{r}_{:,m}$ with $r_{n,m}=|S_{n,m}|^2$) prior to the length-M slow-time Doppler DFT; for i.i.d. $S_{n,m}$, $\mathbb{E}[|\mathcal{A}_{\mathrm{FST}}(k,q)|^2]/(MN^2)=(\kappa_{\mathrm{marg}}-1)/N$ holds at both $q=0$ and $q\neq 0$.

A. The Kurtosis–Capacity Tradeoff Under i.i.d. Signaling

Under i.i.d. symbol signaling, (1) ties $(\kappa_{\mathrm{marg}}-1)/N$ directly to the marginal kurtosis $\kappa_{\mathrm{marg}}=\mathbb{E}[r^2_{n,m}]$:

1) *Constant-Modulus Alphabets ($\kappa_{\mathrm{marg}}=1$):* Phase-shift keying (PSK) sets $r_{n,m}=|S_{n,m}|^2=1$ almost surely, so $\mathrm{Var}(r_{n,m})=\kappa_{\mathrm{marg}}-1=0$ at $q=0$ [6], [8], with $\lim_{\rho\to\infty}[C_{\mathrm{AWGN}}(\rho)-I_{\mathrm{PSK}}(\rho)]=\frac{1}{2}\log_2(\pi e/2)=1.047$ b/s/Hz (1.53 dB SNR gap to $C_{\mathrm{AWGN}}(\rho)=\log_2(1+\rho)$) and $d^2_{\min,2^b\text{-PSK}}=4\sin^2(\pi/2^b)$ ($b>2$).
2) *Gaussian and Probabilistically Shaped Alphabets ($\kappa_{\mathrm{marg}}\in(1.80,2]$):* Capacity $C_{\mathrm{AWGN}}(\rho)$ requires $S_{n,m}\sim\mathcal{CN}(0,1)$ with $r_{n,m}\sim\mathrm{Exp}(1)$ and $\kappa_{\mathrm{marg}}=2$ [11], approximated via Probabilistic Amplitude Shaping (PAS) [12], CCDM [13], or Enumerative Sphere Shaping (ESS) [14], [15]. Under the Maxwell-Boltzmann radial distribution $P(a_m)\propto e^{-\lambda a_m^2}$, $\kappa_{\mathrm{marg}}\in[1.85,1.95]$ and $\mathbb{E}[|\mathcal{A}_{\mathrm{FST}}(k,0)|^2]/(MN^2)=(\kappa_{\mathrm{marg}}-1)/N\in[0.85,0.95]/N$.

Under i.i.d. signaling, $\kappa_{\mathrm{marg}}\in[1,2]$ parameterizes the $(\kappa_{\mathrm{marg}}-1)/N$ vs. $I(S;Y)$ Pareto locus [16]–[18]; reducing $(\kappa_{\mathrm{marg}}-1)/(MN)$ by $10\log_{10}M\in[40,50]$ dB via coherent integration requires $M\in[10^4,10^5]$ symbols [5] ($MT_{\mathrm{sym}}=357$ ms at $\Delta f=30$ kHz, $T_{\mathrm{sym}}=35.7$ μs, vs. 0.125–0.5 ms for one $M=14$ NR slot). Per-subcarrier reciprocal zero-forcing $\tilde{R}_{\mathrm{ZF},n,m}=Y_{n,m}/S_{n,m}$ divides out $|S_{n,m}|^2$ in fast time with noise penalty $\eta_{\mathrm{ZF}}=\mathbb{E}[|S|^{-2}]\geq 3.0$ ($+4.77$ dB on PAS-64QAM) and does not null slow-time multipath internal clutter motion (ICM) $h_\ell[m]$ at $q_t\neq 0$.

The author is with SRH University of Applied Sciences, Berlin, Germany (e-mail: thrinaypotta@gmail.com; thrinay@ieee.org).

TABLE I
COMPARISON OF RANDOM ISAC CONSTELLATION SHAPING AND WAVEFORM STATISTICAL FRAMEWORKS

Ref.	Coupling	κ_{marg}	$\mathbb{E}[\lvert\mathcal{A}_{\mathrm{FST}}(k,0)\rvert^2]/(MN^2)$	$\mathcal{Q}_{\mathrm{null}}$ Nulling	$M=14$	Rate / Gain
[5]	$C_{n,m}=0$ $(n\neq m)$	$[1.0, 2.0]$	$(\kappa_{\mathrm{marg}}-1)/N$	No ($M\sim 10^4$)	No	$\Delta I(\kappa_{\mathrm{marg}})$
[6]	$C_{n,m}=0$ (QAM/PSK)	1.0–1.38	$(\kappa_{\mathrm{marg}}-1)/N$	$q=0$ ($\kappa_{\mathrm{marg}}=1$)	Yes (PSK)	0 dB
[8]	$C_{n,m}=0$ (2D AF)	$[1.0, 2.0]$	$(\kappa_{\mathrm{marg}}-1)/N$	$\mathbf{C}\neq\mathbf{0}$ open [8, Sec. V]	Yes (PSK)	$\Delta I(\kappa_{\mathrm{marg}})$
[16]	$C_{n,m}=0$ (1D PCS)	$[1.0, 2.0]$	$(\kappa_{\mathrm{marg}}-1)/N$	No	Yes	1D Pareto
[12], [13]	$L>10^3$	$[1.85, 1.95]$	$[0.85, 0.95]/N$	No	No ($L\gg 14$)	≤ 1.53 dB
This Work	$\mathbf{C}=\mathrm{Cov}(\mathbf{r})$	$\frac{2M+1-d_{\mathrm{null}}}{M+1}$	$\mathbf{0}$ $(2\sigma^2_{\mathrm{EVM}}/N)$	$\forall q\in\mathcal{Q}_{\mathrm{null}}$	Yes ($M=14$)	**97.7%–98.0%** ($d_{\mathrm{null}}=1$) **93.1%** ($d_{\mathrm{null}}=3$)

B. From Scalar Kurtosis to Structured Fourth-Order Covariance

In Shannon's sphere-packing geometry [11], [14], [19]–[21], uniform signaling on the complex sphere $\mathbf{s}\sim\mathcal{U}(\sqrt{L}\,\mathbb{S}^{2L-1})$ approaches $C_{\mathrm{AWGN}}(\rho)$ as $L\to\infty$ with constant block energy $\|\mathbf{s}\|_2^2=\mathbf{1}_L^T\mathbf{r}=L$. As noted in [8, Sec. V], the discrete AF derivations in [6], [8] assume i.i.d. symbols ($C_{n,m}=0$ for $n\neq m$), leaving non-i.i.d. shaped ensembles $\mathbf{C}=\mathrm{Cov}(\mathbf{r})\neq(\kappa_{\mathrm{marg}}-1)\mathbf{I}$ uncharacterized.

Here the fourth-order moment matrix $\mathbf{S}_{\mathrm{mom}}=\mathbb{E}[(\mathbf{s}^*\otimes\mathbf{s})(\mathbf{s}^*\otimes\mathbf{s})^H]$ of [6], [8] is generalized to non-i.i.d. proper circularly symmetric constellations with covariance $\mathbf{C}=\mathrm{Cov}(\mathbf{r})\in\mathbb{R}^{N\times N}$ ($r_n\triangleq|S_n|^2$):

1) *1D Fast-Time vs. 2D Slow-Time Subspace Orthogonality:* For $\mathbf{s}\sim\mathcal{U}(\sqrt{N}\,\mathbb{S}^{2N-1})$ across N subcarriers ($M=1$), $\mathbf{1}_N^T\mathbf{r}=N$ places only the $k=0$ DC vector $\mathbf{1}_N$ in $\ker(\mathbf{C})$, and negative off-diagonal covariances $C_{n,m}=-(\kappa_{\mathrm{marg}}-1)/(N-1)$ scale $\mathbb{E}[|\tilde{r}_k|^2]/N=\mathbf{f}_k^H\mathbf{C}\mathbf{f}_k$ by $N/(N-1)$ for all $k\neq 0$ (Lemma 1). Shaping along the M slow-time symbols of each subcarrier ($n\in\{0,\ldots,N-1\}$) instead aligns $\mathbf{1}_M^T\mathbf{r}_{n,:}=M$ with the $q=0$ slow-time DFT vector $\mathbf{f}_{M,0}$ across all N subcarriers.
2) *Subspace Clutter-Trench Nulling and Parseval Redistribution:* Projecting $\mathbf{r}_{n,:}-\mathbf{1}_M$ onto $\mathcal{V}_{\mathrm{null}}^{\perp}$ ($\mathbf{V}_{\mathrm{null}}^T(\mathbf{r}_{n,:}-\mathbf{1}_M)=\mathbf{0}$, $d_{\mathrm{null}}=|\mathcal{Q}_{\mathrm{null}}|$) gives $\mathcal{A}_{\mathrm{FST}}(k,q)=0$ almost surely for all $(k,q)\in(\{0,\ldots,N-1\}\times\mathcal{Q}_{\mathrm{null}})\setminus\{(0,0)\}$ in one slot ($M=14$ or 16), with out-of-trench variance $(\kappa_{\mathrm{marg}}-1)M/[N(M-d_{\mathrm{null}})]$ by Parseval's identity $\mathrm{Tr}(\mathbf{C}_{\mathrm{slow}})=M(\kappa_{\mathrm{marg}}-1)$ (Theorem 1).
3) *Single-Slot Finite-Blocklength Capacity Retention:* On $\mathcal{P}_M(\mathcal{Q}_{\mathrm{null}})$, $\kappa_{\mathrm{proj}}(M,d_{\mathrm{null}})=(2M+1-d_{\mathrm{null}})/(M+1)$ (Theorem 2), $\Delta I_{\mathrm{sphere}}(14, 20\text{ dB})=0.1524$ b/s/Hz (97.7% of C_{AWGN}), $\Delta I_{\mathrm{sphere}}(16, 20\text{ dB})=0.1333$ b/s/Hz (98.0%), and $\frac{1}{14}I(\mathbf{S};\mathbf{Y})/C_{\mathrm{AWGN}}=93.1\%$ at $(M,d_{\mathrm{null}})=(14,3)$ (Theorem 3), with $R_{\mathrm{APSK}}(L)=4.0000$ b/s/Hz for $L\in\{7,8\}$ (Proposition 3, Algorithm 1).

C. Summary of Contributions and Paper Organization

Table I compares $\mathbf{C}=\mathrm{Cov}(\mathbf{r})$ against [5], [6], [8], [12], [13], [16]:

- *Section II and Section III:* $\mathbf{S}_{\mathrm{mom}}=\mathbf{I}_{N^2}+\mathbf{S}_1+\mathbf{S}_2+\mathbf{S}_{\mathrm{cov}}$ (4), $\frac{1}{N}\mathbb{E}[|\tilde{r}_k|^2]=\mathbf{f}_k^H\mathbf{C}\mathbf{f}_k$ and $N/(N-1)$ full-sphere factor (Lemma 1), 2D FST-AF nulling and $M/(M-d_{\mathrm{null}})$ Parseval factor (Theorem 1), 1D comb-coupled sub-block variance (Corollary 1), SFFT-OTFS and DAFT-AFDM nulling (Proposition 1), and $\sigma^2_{\mathrm{int}}(q_t)$ and $\mathrm{CRLB}(\hat{\tau}_t)$ under ICM σ_c and EVM σ^2_{EVM} (Proposition 2).
- *Section IV-A,B:* $\kappa_{\mathrm{proj}}(M,d_{\mathrm{null}})=(2M+1-d_{\mathrm{null}})/(M+1)$ and $\kappa_{\mathrm{ret}}(M,d_{\mathrm{null}})=1+\bar{\alpha}_2^2(M-d_{\mathrm{null}})/(M+1)$ on $\mathcal{P}_M(\mathcal{Q}_{\mathrm{null}})$ (Theorem 2), $\Delta I_{\mathrm{sphere}}(L,\rho)=\frac{1}{L}D_{\mathrm{KL}}(f_{R^2_{\mathrm{sph}}}\|f_{R^2_{\mathrm{G}}})$, $\Delta I_{\mathrm{part}}(M,d_{\mathrm{null}},\rho)$, $\mathcal{O}(d_{\mathrm{null}}/M)$ DPI converse, and $N^*_{\mathrm{blk}}(L,\rho,\epsilon)$ (Theorem 3).
- *Section IV-C, Section V, Section VI, and Appendices A–E:* $R_{\mathrm{APSK}}(L)=4.0000$ b/s/Hz for $(n_1,n_2,n_3)=(2,4,2)$ ($L=8$) and $(2,3,2)$ ($L=7$), $d^2_{\mathrm{min,APSK}}=1.84\,d^2_{\mathrm{min,16\text{-}PSK}}$ (+2.65 dB), 3GPP TS 38.211 DMRS pilot pinning, paired half-slot cosets (Proposition 3, Algorithm 1, Remark 1), and $\mathrm{ISLR}_0(\epsilon_D)\approx\sigma^2_{\mathrm{EVM}}/M+\frac{\pi^2}{3M}\epsilon_D^2$.

Notations: For $\mathbf{A}\in\mathbb{C}^{N\times M}$ and $\mathbf{a}\in\mathbb{C}^N$, $\mathbf{A}^T$, $\mathbf{A}^*$, $\mathbf{A}^H$, $\mathbf{A}^\dagger$, $\|\mathbf{A}\|_F$, and $\|\mathbf{a}\|_p$ are transpose, conjugate, Hermitian, pseudoinverse, Frobenius norm, and ℓ_p norm; $\otimes$, $\odot$, $\mathrm{vec}(\mathbf{A})\in\mathbb{C}^{NM}$, $\mathrm{diag}(\mathbf{A})\in\mathbb{C}^N$, and $\mathrm{Diag}(\mathbf{a})\in\mathbb{C}^{N\times N}$ are Kronecker and Hadamard products, column vectorization, diagonal vector, and diagonal matrix; $\mathbf{I}_N$, $\mathbf{1}_N=[1,\ldots,1]^T$, $[\mathbf{F}_N]_{k,n}=N^{-1/2}e^{-j2\pi kn/N}$, $\mathbb{E}[\cdot]$, $\mathrm{Var}(\cdot)$, and $\mathrm{Cov}(\cdot)$ are the $N\times N$ identity, all-ones vector, unitary DFT, expectation, variance, and covariance.

II. SYSTEM MODEL AND PRELIMINARIES

A. Unitary Multicarrier Frame and 1D/2D Ambiguity Functions

An ISAC transmitter radiates a frame of M multicarrier symbols across N subcarriers over bandwidth $B=N\Delta f$ and elementary symbol duration $T=1/\Delta f$. The random data symbol matrix is $\mathbf{S}=[\mathbf{s}_0,\ldots,\mathbf{s}_{M-1}]\in\mathbb{C}^{N\times M}$, with entry $S_{n,m}=[\mathbf{S}]_{n,m}$ on subcarrier $n\in\{0,\ldots,N-1\}$ during slow-time symbol $m\in\{0,\ldots,M-1\}$. Multiplication of column $\mathbf{s}_m\in\mathbb{C}^N$ by a unitary fast-time transform $\mathbf{U}\in\mathbb{C}^{N\times N}$ ($\mathbf{U}^H\mathbf{U}=\mathbf{I}_N$) gives the discrete-time vector $\mathbf{x}_m=\mathbf{U}\mathbf{s}_m=[x_m[0],\ldots,x_m[N-1]]^T\in\mathbb{C}^N$, followed by a cyclic prefix (CP) of length $N_{\mathrm{cp}}\geq k_{\max}$. Setting $\mathbf{U}=\mathbf{F}_N^H$ gives CP-OFDM; $\mathbf{U}=\mathbf{I}_N$ gives single-carrier frequency-domain equalization (SC-FDE); and $\mathbf{U}=\mathbf{\Lambda}_{c_1}^H\mathbf{F}_N^H\mathbf{\Lambda}_{c_2}^H$ with $\mathbf{\Lambda}_{c_i}=\mathrm{Diag}(\exp(-j2\pi c_i n^2))$ gives unitary AFDM [23].

For a single CP-OFDM symbol $\mathbf{x} = \mathbf{F}_N^H \mathbf{s}$, the discrete periodic autocorrelation function (P-ACF) at delay lag $k \in \{0, \dots, N-1\}$ obeys the Wiener-Khinchin identity [6]

$$\tilde{r}_k \triangleq \sum_{n=0}^{N-1} x[n]\, x^*[(n-k) \bmod N] = \sqrt{N}\, \mathbf{f}_k^H \mathbf{r}, \qquad (2)$$

with $\mathbf{r} \triangleq \mathbf{s} \odot \mathbf{s}^* = [|S_0|^2, \dots, |S_{N-1}|^2]^T \in \mathbb{R}_{\geq 0}^N$ and $[\mathbf{f}_k]_n = N^{-1/2} e^{j2\pi kn/N}$ ($\mathbf{f}_k \triangleq \mathbf{F}_N^H \mathbf{e}_k$). Over $M \in \{14, 16\}$ symbols [14], $\tilde{r}_{k,m} = \sqrt{N}\, \mathbf{f}_{N,k}^H \mathbf{r}_{:,m}$ removes $\phi_{n,m}$ prior to $\mathbf{F}_M$ [8], [10]. For $\epsilon_D \triangleq f_D T_{\mathrm{sym}} \ll 1$, the 2D Fast-Time/Slow-Time Ambiguity Function (2D FST-AF) at $(k, q) \in \{0, \dots, N-1\} \times \{-M/2, \dots, M/2-1\}$ is

$$\begin{aligned} \mathcal{A}_{\mathrm{FST}}(k, q) &\triangleq \sum_{m=0}^{M-1} \tilde{r}_{k,m}\, e^{-j\frac{2\pi qm}{M}} = \sqrt{NM}\, \mathbf{f}_{N,k}^H \mathbf{R}\, \mathbf{f}_{M,q}^* \\ &= \sum_{n=0}^{N-1} \sum_{m=0}^{M-1} r_{n,m}\, e^{j\frac{2\pi kn}{N}} e^{-j\frac{2\pi qm}{M}}, \end{aligned} \qquad (3)$$

where $\mathbf{R} \in \mathbb{R}_{\geq 0}^{N \times M}$ has entries $r_{n,m} \triangleq |S_{n,m}|^2$, and $\mathbf{f}_{N,k} \in \mathbb{C}^N$, $\mathbf{f}_{M,q} \in \mathbb{C}^M$ are the unitary IDFT columns of lengths N and M.

B. Statistical Assumptions and Fourth-Order Moment Matrix

Non-i.i.d. amplitude-shaped constellations are modeled under the following phase-symmetry assumption.

Assumption 1 (Unit Power, Properness, and Circular Phase Symmetry): Every symbol $S_{n,m} = \sqrt{r_{n,m}}\, e^{j\phi_{n,m}}$ in $\mathbf{S} \in \mathbb{C}^{N \times M}$ has unit mean intensity $\mathbb{E}[r_{n,m}] = \mathbb{E}[|S_{n,m}|^2] = 1$. The phases $\{\phi_{n,m}\}$ are mutually i.i.d., independent of the intensity matrix $\mathbf{R} = [r_{n,m}]$, and follow a U-fold rotationally symmetric law ($U \geq 4$, e.g., uniform $\mathcal{U}[0, 2\pi)$ or Gray-coded QPSK/2^b-PSK), so that $\mathbb{E}[S_{n,m}] = \mathbb{E}[S_{n,m}^2] = \mathbb{E}[S_{n,m}^3] = 0$.

Under Assumption 1, $\phi_{n,m} \in [0, 2\pi)$ are i.i.d. across (n, m) and $\mathbf{r}_{n,:} = [r_{n,0}, \dots, r_{n,M-1}]^T \in \mathbb{R}_{\geq 0}^M$ is coupled over blocks of length $L \leq M$.

Definition 1 (Marginal Kurtosis, Intensity Covariance Matrix $\mathbf{C}$, and Fourth-Order Moment Matrix $\mathbf{S}_{\mathrm{mom}}$): For any random symbol vector $\mathbf{s} \in \mathbb{C}^N$ satisfying Assumption 1 with identical marginal intensity distributions across indices $n \in \{0, \dots, N-1\}$:

1) The *marginal fourth-order kurtosis* is $\kappa_{\mathrm{marg}} \triangleq \mathbb{E}[|S_n|^4] = \mathbb{E}[r_n^2] \geq 1$, so that each marginal intensity variance is $\mathrm{Var}(r_n) = \kappa_{\mathrm{marg}} - 1$.

2) The *symbol-intensity covariance matrix* is $\mathbf{C} \triangleq \mathrm{Cov}(\mathbf{r}) = \mathbb{E}[(\mathbf{r} - \mathbf{1}_N)(\mathbf{r} - \mathbf{1}_N)^T] \in \mathbb{R}^{N \times N}$, whose diagonal entries are $C_{n,n} = \kappa_{\mathrm{marg}} - 1$ and off-diagonal entries are $C_{n,m} = \mathrm{Cov}(r_n, r_m)$ for $n \neq m$.

3) Let $\tilde{\mathbf{s}} \triangleq \mathrm{vec}(\mathbf{s}\mathbf{s}^H) = \mathbf{s}^* \otimes \mathbf{s} \in \mathbb{C}^{N^2}$. Under Assumption 1, $\mathbb{E}[S_{n_1}^* S_{n_2} S_{n_3} S_{n_4}^*]$ vanishes unless $\{n_1, n_4\} = \{n_2, n_3\}$, where $\mathbb{E}[|S_n|^2 |S_m|^2] = 1 + C_{n,m}$ ($n \neq m$). Collecting the unit-mean part of ($n_1 = n_3 = n$, $n_2 = n_4 = m$) into $\mathbf{I}_{N^2} = \sum_{n,m} (\mathbf{e}_n \mathbf{e}_n^T \otimes \mathbf{e}_m \mathbf{e}_m^T)$ and that of ($n_1 = n_2 = n \neq m = n_3 = n_4$) into $\mathbf{S}_2$, the $N^2 \times N^2$ *fourth-order moment matrix* $\mathbf{S}_{\mathrm{mom}} \triangleq \mathbb{E}[\tilde{\mathbf{s}}\tilde{\mathbf{s}}^H]$ decomposes as

$$\mathbf{S}_{\mathrm{mom}} = \mathbf{I}_{N^2} + \mathbf{S}_1 + \mathbf{S}_2 + \mathbf{S}_{\mathrm{cov}}, \qquad (4)$$

where $\mathbf{S}_1 \triangleq \sum_{n=0}^{N-1} (\kappa_{\mathrm{marg}} - 2)(\mathbf{e}_n \mathbf{e}_n^T \otimes \mathbf{e}_n \mathbf{e}_n^T)$, $\mathbf{S}_2 \triangleq \sum_{n \neq m} (\mathbf{e}_n \mathbf{e}_m^T \otimes \mathbf{e}_n \mathbf{e}_m^T) = \mathrm{vec}(\mathbf{I}_N)\mathrm{vec}(\mathbf{I}_N)^T - \sum_{n=0}^{N-1} (\mathbf{e}_n \mathbf{e}_n^T \otimes \mathbf{e}_n \mathbf{e}_n^T)$, and $\mathbf{S}_{\mathrm{cov}} \triangleq \sum_{n \neq m} C_{n,m} (\mathbf{e}_n \mathbf{e}_m^T \otimes \mathbf{e}_n \mathbf{e}_m^T + \mathbf{e}_n \mathbf{e}_m^T \otimes \mathbf{e}_m \mathbf{e}_m^T)$ collects both non-i.i.d. radial covariance pairings.

For i.i.d. constellations, $C_{n,m} = 0$ for all $n \neq m$ ($\mathbf{S}_{\mathrm{cov}} = \mathbf{0}$), and (4) reduces to the i.i.d. moment matrix of [6, Appendix A, Lemma 2] and [8, Appendix A, Eq. (106)]. For non-i.i.d. ensembles ($\mathbf{S}_{\mathrm{cov}} \neq \mathbf{0}$), $C_{n,m}$ controls the delay-Doppler sidelobe variance while $\kappa_{\mathrm{marg}} = 1 + C_{n,n}$ remains near 2.

III. Statistical Characterization and Subspace Clutter-Trench Nulling

A. 1D Fast-Time Spectral-Covariance Identity and the $N/(N-1)$ Full-Sphere Penalty

For a single multicarrier symbol $\mathbf{x} = \mathbf{U}\mathbf{s}$ and circular shift matrix $\mathbf{J}_k$ ($[\mathbf{J}_k]_{n,m} = 1$ if $(n - m) \bmod N = k$), the P-ACF at lag k is $\tilde{r}_k = \mathbf{s}^H \mathbf{D}_k \mathbf{s} = \mathrm{vec}(\mathbf{D}_k)^H \tilde{\mathbf{s}}$ with $\mathbf{D}_k \triangleq \mathbf{U}^H \mathbf{J}_k \mathbf{U}$. Evaluating $\mathbb{E}[|\tilde{r}_k|^2] = \mathrm{vec}(\mathbf{D}_k)^H \mathbf{S}_{\mathrm{mom}} \mathrm{vec}(\mathbf{D}_k)$ via (4) yields Lemma 1.

Lemma 1 (1D Spectral-Covariance Ranging Sidelobe Identity and the $N/(N-1)$ Fast-Time Sidelobe Penalty): Let $\mathbf{s} \in \mathbb{C}^N$ be a random frequency-domain symbol vector satisfying Assumption 1 and Definition 1. Then:

(a) General Unitary Multicarrier Variance Identity: For any unitary $\mathbf{U} \in \mathbb{C}^{N \times N}$ and any non-zero delay lag $k \in \{1, \dots, N-1\}$ ($\mathrm{Tr}(\mathbf{D}_k) = 0$),

$$\begin{aligned} \mathbb{E}\Big[|\tilde{r}_k|^2\Big] &= N + (\kappa_{\mathrm{marg}} - 2) \sum_{n=0}^{N-1} |[\mathbf{D}_k]_{n,n}|^2 \\ &\quad + \sum_{n \neq m} C_{n,m} \Big([\mathbf{D}_k]_{n,n}^* [\mathbf{D}_k]_{m,m} + |[\mathbf{D}_k]_{n,m}|^2 \Big). \end{aligned} \qquad (5)$$

(b) CP-OFDM Spectral-Covariance Identity: For CP-OFDM ($\mathbf{U} = \mathbf{F}_N^H$), $\mathbf{D}_k = \sqrt{N}\,\mathrm{Diag}(\mathbf{f}_k^*)$ is diagonal ($|[\mathbf{D}_k]_{n,n}|^2 = 1$), so (5) simplifies for all $k \in \{0, \dots, N-1\}$ to

$$\frac{1}{N}\mathbb{E}\Big[|\tilde{r}_k|^2\Big] = \underbrace{N\,\delta[k]}_{\substack{\text{Deterministic} \\ \text{Iceberg}}} + \underbrace{\mathbf{f}_k^H \mathbf{C}\, \mathbf{f}_k}_{\substack{\text{Shaped Radial-Covariance} \\ \text{Sea Level}}}. \qquad (6)$$

Consequently, $\mathbb{E}[|\tilde{r}_k|^2] = 0$ (and $\tilde{r}_k = 0$ almost surely) at lag $k \neq 0$ if and only if $\mathbf{f}_k \in \ker(\mathbf{C})$.

(c) 1D Fast-Time vs. 2D Slow-Time Subspace Orthogonality ($\frac{N}{N-1}$ Fast-Time Sidelobe Penalty): If $\mathbf{s}$ is drawn from any 1D exchangeable constant-energy shell across the N subcarriers ($\|\mathbf{s}\|_2^2 = \mathbf{1}_N^T \mathbf{r} = N$ almost surely, $C_{n,m} = c_{\mathrm{off}}$ for $n \neq m$), then $\mathbf{C}\mathbf{1}_N = \mathbf{0}$ forces $c_{\mathrm{off}} = -(\kappa_{\mathrm{marg}} - 1)/(N-1) < 0$ and $\mathbf{C} = \frac{N(\kappa_{\mathrm{marg}}-1)}{N-1}(\mathbf{I}_N - \frac{1}{N}\mathbf{1}_N\mathbf{1}_N^T)$. Since $\mathbf{f}_k \perp \mathbf{1}_N$ for all $k \neq 0$,

$$\frac{1}{N}\mathbb{E}\Big[|\tilde{r}_k|^2\Big] = \mathbf{f}_k^H \mathbf{C}\, \mathbf{f}_k = \frac{N}{N-1}(\kappa_{\mathrm{marg}} - 1), \quad \forall k \neq 0. \qquad (7)$$

For uniform signaling on $\sqrt{N}\,\mathbb{S}^{2N-1}$ ($\kappa_{\mathrm{marg}} = 2N/(N+1)$), $\frac{1}{N}\mathbb{E}[|\tilde{r}_k|^2] = \frac{N}{N+1} \to 1$ (0 dB), providing zero sidelobe suppression relative to i.i.d. Gaussian signaling.

Proof: See Appendix A. ∎

B. 2D Slow-Time Clutter-Trench Nulling and Parseval Redistribution

In $\mathbf{S} \in \mathbb{C}^{N\times M}$, delay lag k is dual to subcarrier index n and Doppler bin q is dual to slow-time symbol index m. Coupling $r_{n,m}$ across $m \in \{0,\dots,M-1\}$ puts selected slow-time DFT columns $\mathbf{f}_{M,q}$ into $\ker(\mathbf{C}_{\text{slow}})$ and nulls all $k \in \{1,\dots,N-1\}$ on those Doppler bins. For $\mathcal{Q}_{\text{null}} = \{-Q_c,\dots,Q_c\} \subset \{-M/2,\dots,M/2-1\}$ of size $d_{\text{null}} \triangleq |\mathcal{Q}_{\text{null}}| = 2Q_c+1 < M$, let $\mathbf{V}_{\text{null}} \in \mathbb{R}^{M\times d_{\text{null}}}$ be an orthonormal basis of

$$\mathcal{V}_{\text{null}} \triangleq \operatorname{span}\Big\{\mathbf{1}_M,\ \big\{\cos(2\pi qm/M),\ \sin(2\pi qm/M)\big\}_{q=1}^{Q_c}\Big\} \subset \mathbb{R}^M, \quad (8)$$

with projectors $\mathbf{P}_{\text{null}} \triangleq \mathbf{V}_{\text{null}}\mathbf{V}_{\text{null}}^T$ and $\mathbf{P}_\perp \triangleq \mathbf{I}_M - \mathbf{P}_{\text{null}}$.

Theorem 1 (2D Slow-Time Clutter-Trench Ambiguity Nulling, Parseval Redistribution, and 1D Subspace Spectral Nulling): Let $\mathbf{S} \in \mathbb{C}^{N\times M}$ satisfy Assumption 1.

(a) 2D Slow-Time Clutter-Trench Nulling and Parseval Variance Redistribution: If the rows $\{\mathbf{r}_{n,:}\}_{n=0}^{N-1}$ are mutually independent with $\mathbf{V}_{\text{null}}^T(\mathbf{r}_{n,:} - \mathbf{1}_M) = \mathbf{0}$ almost surely and

$$\mathbf{C}_{\text{slow}} \triangleq \operatorname{Cov}(\mathbf{r}_{n,:}) = \frac{M(\kappa_{\text{marg}}-1)}{M-d_{\text{null}}}\,\mathbf{P}_\perp, \quad (9)$$

then for all $k \in \{0,\dots,N-1\}$ and $q \in \{-M/2,\dots,M/2-1\}$,

$$\frac{1}{MN^2}\mathbb{E}\Big[\big|\mathcal{A}_{\text{FST}}(k,q)\big|^2\Big] = \underbrace{M\,\delta[k]\,\delta[q]}_{\substack{\text{Deterministic}\\ \text{Mainlobe Iceberg}}} + \begin{cases} \underbrace{0,}_{\substack{\text{Clutter-Trench Sea Level}\\ \text{(Zero Variance in } \mathcal{Q}_{\text{null}})}} & \text{if } q \in \mathcal{Q}_{\text{null}}, \\ \underbrace{\dfrac{\kappa_{\text{marg}}-1}{N}\left(\dfrac{M}{M-d_{\text{null}}}\right)}_{\substack{\text{Parseval Out-of-Trench}\\ \text{Variance Redistribution}}}, & \text{if } q \notin \mathcal{Q}_{\text{null}}. \end{cases} \quad (10)$$

Thus $\mathcal{A}_{\text{FST}}(k,q) = 0$ almost surely for all $(k,q) \in (\{0,\dots,N-1\}\times\mathcal{Q}_{\text{null}}) \setminus \{(0,0)\}$ (both $k \neq 0, q \in \mathcal{Q}_{\text{null}}$ and $k = 0, q \in \mathcal{Q}_{\text{null}} \setminus \{0\}$), and $\sum_q \mathbf{f}_{M,q}^H \mathbf{C}_{\text{slow}} \mathbf{f}_{M,q} = \operatorname{Tr}(\mathbf{C}_{\text{slow}}) = M(\kappa_{\text{marg}}-1)$.

(b) 1D Subspace Spectral-Nulling Shell ($M = 1$): Within a single OFDM symbol ($M = 1$), let $\mathcal{K}_{\text{null}} \subset \{1,\dots,\lfloor N/2\rfloor\}$ be a set of $K_{\text{null}} = |\mathcal{K}_{\text{null}}|$ ranging lags with real Fourier basis $\mathbf{V}_{\text{1D}} \in \mathbb{R}^{N\times(2K_{\text{null}}+1)}$ spanning $\{\mathbf{1}_N, \{\cos(2\pi kn/N), \sin(2\pi kn/N)\}_{k\in\mathcal{K}_{\text{null}}}\}$. If $\mathbf{r} \in \mathbb{R}_{\geq 0}^N$ satisfies $\mathbf{V}_{\text{1D}}^T(\mathbf{r} - \mathbf{1}_N) = \mathbf{0}$ almost surely with isotropic covariance on $\operatorname{range}(\mathbf{V}_{\text{1D}})^\perp$, then

$$\frac{\mathbb{E}\big[|\tilde{r}_k|^2\big]}{N} = \begin{cases} 0, & \min(k, N-k) \in \mathcal{K}_{\text{null}}, \\ \frac{N(\kappa_{\text{marg}}-1)}{N-2K_{\text{null}}-1}, & \text{otherwise } (k \neq 0). \end{cases} \quad (11)$$

Proof: See Appendix B. ∎

When $d_{\text{null}} = 1$ ($\mathcal{Q}_{\text{null}} = \{0\}$), $\mathbf{V}_{\text{null}}^T(\mathbf{r}_{n,:} - \mathbf{1}_M) = 0$ simplifies to the constant block-energy shell $\sum_{m=0}^{L-1} |S_{n,m}|^2 = L$ ($M = L$ or $2L$). In 1D fast time, coupling intensities along $B = N/L$ interleaved comb sub-blocks gives Corollary 1.

Corollary 1 (1D Comb-Coupled Sub-Block Spherical Shaping): For $B = N/L$ residue combs $\mathcal{I}_b = \{b + lB : l \in \{0,\dots,L-1\}\}$ ($b \in \{0,\dots,B-1\}$) with $r_{b+lB} = \bar{r}_b$, $\bar{\mathbf{r}} = [\bar{r}_0,\dots,\bar{r}_{B-1}]^T$ on $\mathbf{1}_B^T\bar{\mathbf{r}} = B$, and $\kappa_{\text{marg}} = \mathbb{E}[\bar{r}_b^2]$ under Assumption 1, $\mathbf{r} - \mathbf{1}_N \in \operatorname{span}\{\mathbf{f}_{mL}\}_{m=1}^{B-1}$ and $\mathbf{f}_k \in \ker(\mathbf{C})$ for $k \bmod L \neq 0$:

$$\frac{1}{N}\mathbb{E}\Big[|\tilde{r}_k|^2\Big] = \begin{cases} 0, & k \bmod L \neq 0, \\ \dfrac{L\,B(\kappa_{\text{marg}}-1)}{B-1}, & k \bmod L = 0\ (k \neq 0). \end{cases} \quad (12)$$

Thus $\tilde{r}_k = 0$ almost surely for $k \in \{1,\dots,L-1\}$.[1]

Proof: Substituting $r_{b+lB} = \bar{r}_b$ into (2) factors $\tilde{r}_k = \sum_{b=0}^{B-1} \bar{r}_b e^{j2\pi kb/N} \sum_{l=0}^{L-1} e^{j2\pi kl/L}$. Whenever $k \bmod L \neq 0$, the inner geometric sum vanishes ($\tilde{r}_k = 0$ almost surely). When $k = mL \neq 0$ ($m \in \{1,\dots,B-1\}$), the inner sum equals L, and $\tilde{r}_{mL} = L\sqrt{B}\,\mathbf{f}_{B,m}^H\bar{\mathbf{r}}$ has variance $\mathbb{E}[|\tilde{r}_{mL}|^2]/N = \frac{L^2B}{N}\frac{B(\kappa_{\text{marg}}-1)}{B-1} = \frac{LB(\kappa_{\text{marg}}-1)}{B-1}$ by Lemma 1(c). ∎

C. Extension to Delay-Doppler Waveforms (AFDM/OTFS) and Clutter-Masked Sensing Bounds

Delay-Doppler and chirp waveforms such as AFDM [9], [23], [24] and OTFS [25], [26] modulate symbols via the unitary discrete affine Fourier transform (DAFT/DCFT) or symplectic finite Fourier transform (SFFT). Unprecoded i.i.d. delay-Doppler QAM symbols mix via the inverse SFFT into near-Gaussian frequency-time (FT) envelopes; however, applying slow-time clutter-trench shaping to the FT envelope $\mathbf{S}_{\text{FT}} \in \mathbb{C}^{N\times M}$ (SFFT-precoded OTFS $\mathbf{S}_{\text{DD}} = \mathbf{F}_N^H\mathbf{S}_{\text{FT}}\mathbf{F}_M$) or directly to the native DAFT symbol intensities in AFDM maintains zero-variance clutter-trench nulling at a pulse-Doppler FST matched-filter receiver (per-symbol fast-time correlation followed by a slow-time Doppler DFT, as opposed to uncompensated 2D delay-Doppler correlation).

Proposition 1 (Pulse-Doppler FST Matched-Filter Nulling for FT-Precoded OTFS and Native DAFT-Shaped AFDM): Let $\mathbf{R} = [r_{n,m}] \in \mathbb{R}_{\geq 0}^{N\times M}$ satisfy Theorem 1(a) at a pulse-Doppler FST matched-filter radar receiver.

(a) FT-Envelope-Shaped (SFFT-Precoded) OTFS: For $\mathbf{S}_{\text{FT}} \in \mathbb{C}^{N\times M}$ with $|S_{\text{FT},n,m}|^2 = r_{n,m}$, $\mathbf{S}_{\text{DD}} \triangleq \mathbf{F}_N^H\mathbf{S}_{\text{FT}}\mathbf{F}_M$, and $\mathbf{x}_m = \mathbf{F}_N^H\mathbf{s}_{\text{FT},m}$, $\mathcal{A}_{\text{OTFS}}(k,q) \triangleq \sum_{m=0}^{M-1}\tilde{r}_{k,m}e^{-j2\pi qm/M} = \sqrt{NM}\,\mathbf{f}_{N,k}^H\mathbf{R}\mathbf{f}_{M,q}^* = 0$ almost surely for all $k \in \{1,\dots,N-1\}$ and $q \in \mathcal{Q}_{\text{null}}$.

(b) Native DAFT-Domain-Shaped AFDM: For $\mathbf{S}_{\text{DAFT}} \in \mathbb{C}^{N\times M}$ with $|S_{\text{DAFT},n,m}|^2 = r_{n,m}$ and $\mathbf{x}_m = \mathbf{\Lambda}_{c_1}^H\mathbf{F}_N^H\mathbf{\Lambda}_{c_2}^H\mathbf{s}_{\text{DAFT},m}$ ($\mathbf{\Lambda}_{c_i} = \operatorname{Diag}(e^{-j2\pi c_i n^2})$, $|\Lambda_{c_2,n,n}|^2 = 1$), $\mathbf{s}_{\text{FT},m} \triangleq \mathbf{\Lambda}_{c_2}^H\mathbf{s}_{\text{DAFT},m}$ satisfies $|S_{\text{FT},n,m}|^2 = r_{n,m}$. Under de-chirped correlation $\tilde{r}_{k,m}^{\text{AFDM}} \triangleq \sum_{n=0}^{N-1} x_m[n]\,x_m^*[(n-k) \bmod N]\,e^{-j2\pi c_1(n^2-((n-k) \bmod N)^2)}$, $e^{-j2\pi c_1 k^2}\mathcal{A}_{\text{AFDM}}(k,q) = \sqrt{NM}\,\mathbf{f}_{N,(1-2Nc_1)k \bmod N}^H\mathbf{R}\mathbf{f}_{M,q}^* = 0$ almost surely for all $k \in \{1,\dots,N-1\}$ and $q \in \mathcal{Q}_{\text{null}}$ whenever $2Nc_1 \in \mathbb{Z}$ and $\gcd(1-2Nc_1, N) = 1$.

Proof: From $|S_{\text{FT},n,m}|^2 = r_{n,m}$, $\tilde{r}_{k,m} = \sqrt{N}\,\mathbf{f}_{N,k'}^H\mathbf{r}_{:,m}$ and $\sum_{m=0}^{M-1}\tilde{r}_{k,m}e^{-j2\pi qm/M} = \sqrt{NM}\,\mathbf{f}_{N,k'}^H\mathbf{R}\mathbf{f}_{M,q}^*$ with $k' =$

[1] Under B independent L-spheres $\sum_{n\in\mathcal{I}_b} r_n = L$, $\mathbf{f}_{k,\mathcal{I}_b}$ is constant across $l \in \{0,\dots,L-1\}$ for $k \bmod B = 0$, nulling $k \in \{B, 2B,\dots,(L-1)B\}$ ($B = L = \sqrt{N} = 8$ for $N = 64$ in Fig. 1(a)).

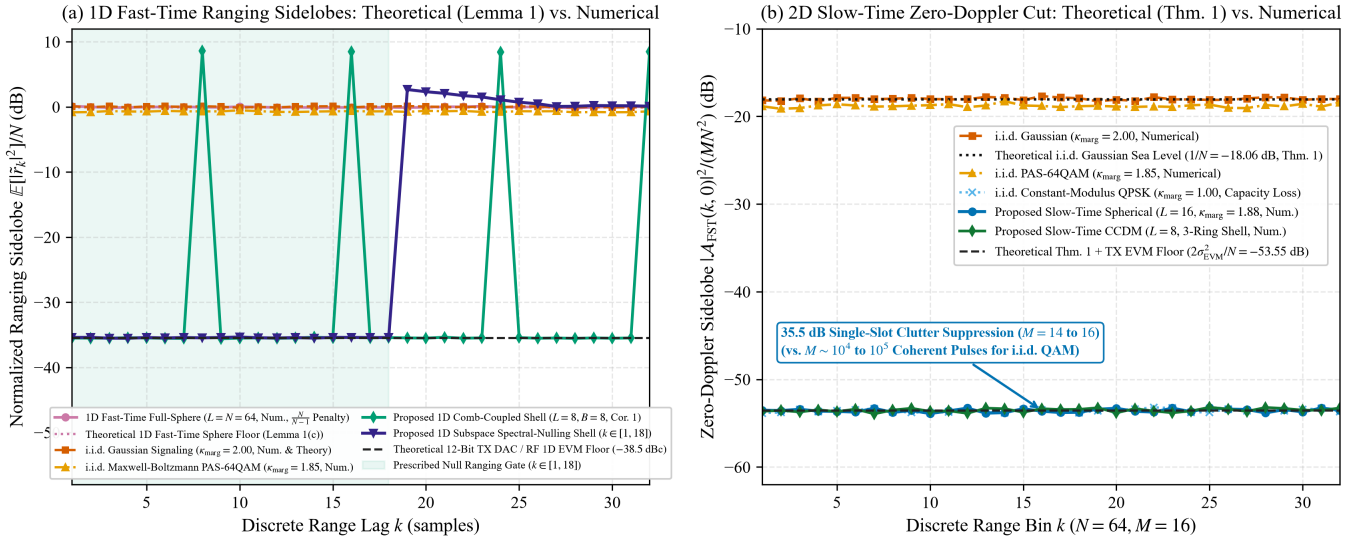


Fig. 1. Theoretical vs. numerical 1D and 2D ranging sidelobe variance ($N = 64$, 12-bit TX DAC, EVM $= -38.5$ dBc). (a) 1D fast-time ranging sidelobes $\mathbb{E}[|\tilde{r}_k|^2]/N$, verifying the $\frac{N}{N-1}$ full-sphere penalty (Lemma 1(c)), comb-interleaved nulling (Corollary 1), and 1D subspace nulling over $k \in [1, 18]$ (Theorem 1(b)). (b) 2D slow-time zero-Doppler ($q = 0$) ambiguity cut $|\mathcal{A}_{\text{FST}}(k, 0)|^2/(MN^2)$, confirming 35.5 dB single-slot suppression to the hardware floor $2\sigma^2_{\text{EVM}}/N = -53.55$ dB.

$k \in \{1, \ldots, N-1\}$ (OTFS) or $k' = (1-2Nc_1)k \bmod N \neq 0$ (AFDM); by Theorem 1(a), $\mathbf{R}\mathbf{f}^*_{M,q} = \mathbf{0}$ for all $q \in \mathcal{Q}_{\text{null}} \setminus \{0\}$. ■

Proposition 2 (Multipath Clutter-Masked SCNR, Delay CRLB, and Hardware Floor): Let $Y_{n,m}$ contain a target return at (τ_t, q_t) ($k_t \neq 0, q_t \neq 0, |\alpha_t|^2 = P_t$), K_c clutter taps $\{\tau_{c,\ell}\}_{\ell=1}^{K_c}$ ($k_{c,\ell} \neq k_t, q_c = 0, P_c = \sum_{\ell=1}^{K_c} \mathbb{E}[|\alpha_{c,\ell}|^2] \gg P_t$) with independent tap phases and unit-power slow-time Gaussian ICM $h_\ell[m]$ ($\sigma_c \ll 1$), AWGN σ_z^2, and TX EVM $\sigma^2_{\text{EVM}} \ll 1$.

(a) Interference Variance $\sigma^2_{\text{int}}(q_t)$ at (k_t, q_t): With target peak $|\mathcal{A}_{\text{FST}}(k_t, q_t)|^2 = (NM)^2 P_t$ (including $q_t \in \mathcal{Q}_{\text{null}} \setminus \{0\}$) and unit per-symbol noise gain, the per-subcarrier interference variance at (k_t, q_t) is

$$\sigma^2_{\text{int}}(q_t) = \sigma_z^2 + P_c\, \eta_{\text{leak}}(q_t, \sigma_c) + P_c \left(\frac{\kappa_{\text{marg}} - 1}{N}\, \xi_{\text{mod}}(q_t) + \frac{2\sigma^2_{\text{EVM}}}{N} \right), \tag{13}$$

with clutter-peak-normalized floor $\frac{\sigma^2_{\text{int}}(q_t)}{MP_c} = \frac{\sigma_z^2}{MP_c} + \frac{\eta_{\text{leak}}(q_t,\sigma_c)}{M} + \frac{\kappa_{\text{marg}}-1}{MN}\xi_{\text{mod}}(q_t) + \frac{2\sigma^2_{\text{EVM}}}{MN}$. Here $\eta_{\text{leak}}(q_t, \sigma_c) \triangleq \beta_{\text{off}}(k_t)\, \mathbb{E}[|H_\ell[q_t]|^2] = \beta_{\text{off}}(k_t)\, \mathcal{O}((\pi\sigma_c)^{2|q_t|})$ with Dirichlet factor

$$\beta_{\text{off}}(k_t) \triangleq \sum_{\ell=1}^{K_c} \frac{\mathbb{E}[|\alpha_{c,\ell}|^2]}{P_c} \left| \frac{1}{N} \sum_{n=0}^{N-1} e^{j2\pi n(k_t/N - \Delta f \tau_{c,\ell})} \right|^2 \in [0, 1)$$

($\beta_{\text{off}}(k_t) = 0$ for integer taps), and $\xi_{\text{mod}}(q_t) \triangleq (\kappa_{\text{marg}} - 1)^{-1} \sum_q \mathbb{E}[|H_\ell[q]|^2]\, \mathbf{f}^H_{M,q_t-q} \mathbf{C}_{\text{slow}} \mathbf{f}_{M,q_t-q}$. For i.i.d. symbols, $\xi_{\text{mod}}(q_t) = 1$; for $d_{\text{null}} = 1$ ($\mathcal{Q}_{\text{null}} = \{0\}$) at $q_t = 1 \notin \{0\}$, $\xi_{\text{mod}}(1) \approx M/(M-1) > 1$ since $q_t - 0 = 1 \notin \mathcal{Q}_{\text{null}}$; for $Q_c \geq |q_t|$ (e.g., $d_{\text{null}} = 3, \mathcal{Q}_{\text{null}} = \{0, \pm 1\}$ at $q_t = \pm 1$), $q_t \in \mathcal{Q}_{\text{null}} \setminus \{0\}$ gives $\mathbf{f}_{M,q_t} \in \ker(\mathbf{C}_{\text{slow}})$, so $\xi_{\text{mod}}(q_t) = 0$ at $\sigma_c = 0$ and $\mathcal{O}((\pi\sigma_c)^{2(Q_c - |q_t|+1)})$ at $\sigma_c > 0$.

(b) Doppler-Conditioned Linear-Covariance (Gaussian-Interference) Delay Fisher Information and CRLB: With mean-square radian bandwidth $B^2_{\text{rms}} \triangleq \frac{4\pi^2 \Delta f^2}{N} \sum_{n=-N/2}^{N/2-1} n^2 = \frac{\pi^2 B^2 (N^2-1)}{3N^2}$ and per-subcarrier interference variance $\sigma^2_{\text{int}}(q_t)/M$ at Doppler bin q_t, the linear-covariance Slepian-Bangs delay CRLB is

$$\begin{aligned} \text{CRLB}(\hat{\tau}_t) &= \frac{\sigma^2_{\text{int}}(q_t)}{2MNP_t B^2_{\text{rms}}} \\ &= \text{CRLB}_{\text{free}}(\hat{\tau}_t) \left(1 + \frac{\text{CNR}}{N}\, \Psi_{\text{mask}}(q_t) \right), \end{aligned} \tag{14}$$

where $\text{CRLB}_{\text{free}}(\hat{\tau}_t) \triangleq \sigma_z^2/(2MNP_t B^2_{\text{rms}})$, $\text{CNR} \triangleq P_c/\sigma_z^2$, and $\Psi_{\text{mask}}(q_t) \triangleq (\kappa_{\text{marg}} - 1)\xi_{\text{mod}}(q_t) + N\eta_{\text{leak}}(q_t, \sigma_c) + 2\sigma^2_{\text{EVM}}$ (exact for slow-time shaped frames where $M^{-1} \sum_{m=0}^{M-1} r_{n,m} = 1$ almost surely on every subcarrier in the dense non-co-located Rayleigh multipath limit $K_c \gg 1$ with $\tau_{c,\ell} \neq \tau_t$, and a conditional-mean analytical benchmark for finite-K_c clutter and i.i.d. baselines).

Proof: See Appendix C. ■

IV. Subspace-Simplex Polytope Geometry, Information-Theoretic Bounds, and Transceiver Design

A. Geometry and Marginal Kurtosis of the Clutter-Trench Polytope

By Theorem 1, admissible slow-time intensity vectors $\mathbf{r} = \mathbf{r}_{n,:} \in \mathbb{R}^M_{\geq 0}$ form the bounded $(M - d_{\text{null}})$-dimensional convex polytope

$$\mathcal{P}_M(\mathcal{Q}_{\text{null}}) \triangleq \left\{ \mathbf{r} \in \mathbb{R}^M_{\geq 0} : \mathbf{V}^T_{\text{null}}(\mathbf{r} - \mathbf{1}_M) = \mathbf{0} \right\}. \tag{15}$$

Theorem 2 characterizes the marginal fourth-order kurtosis $\kappa_{\text{marg}} = \mathbb{E}[r_m^2]$ over $\mathcal{P}_M(\mathcal{Q}_{\text{null}})$.

Theorem 2 (Projected Dirichlet-Simplex Marginal Kurtosis over the Clutter-Trench Polytope): Let $\mathbf{s} \in \mathbb{C}^M$ satisfy Assumption 1 with intensity vector $\mathbf{r} \in \mathcal{P}_M(\mathcal{Q}_{\text{null}})$ ($1 \leq d_{\text{null}} < M$).

(a) Pure Slow-Time Spherical Shaping ($d_{\mathrm{null}}=1$, $\mathcal{Q}_{\mathrm{null}}=\{0\}$): Here $\mathcal{P}_M(\{0\})=M\Delta^{M-1}$. Under uniform spherical signaling $\mathbf{s}\sim\mathcal{U}(\sqrt{M}\,\mathbb{S}^{2M-1})$, $M^{-1}\mathbf{r}\sim\mathrm{Dir}(\mathbf{1}_M)$, and for all $M\geq 2$,

$$\kappa_{\mathrm{marg}}(M)=\frac{2M}{M+1}=2-\frac{2}{M+1},\qquad \mathbf{C}_{\mathrm{slow}}=\frac{M}{M+1}\left(\mathbf{I}_M-\frac{1}{M}\mathbf{1}_M\mathbf{1}_M^T\right). \tag{16}$$

(b) Multi-Bin Clutter-Trench Subspace Shaping ($1\leq d_{\mathrm{null}}<M$): For $\mathbf{u}\sim M\,\mathrm{Dir}(\mathbf{1}_M)$, the orthogonally projected vector $\mathbf{1}_M+\mathbf{P}_\perp(\mathbf{u}-\mathbf{1}_M)$ has isotropic covariance $\frac{M}{M+1}\mathbf{P}_\perp$ on $\mathcal{V}_{\mathrm{null}}^\perp$ and un-clipped second moment (an upper bound on $\mathcal{P}_M(\mathcal{Q}_{\mathrm{null}})$)

$$\kappa_{\mathrm{proj}}(M,d_{\mathrm{null}})=1+\frac{M-d_{\mathrm{null}}}{M+1}=\frac{2M+1-d_{\mathrm{null}}}{M+1}. \tag{17}$$

Under radial retraction $\mathbf{r}=\mathbf{1}_M+\alpha(\mathbf{u})\,\mathbf{P}_\perp(\mathbf{u}-\mathbf{1}_M)\in\mathcal{P}_M(\mathcal{Q}_{\mathrm{null}})$ with step factor $\alpha(\mathbf{u})=\min\{1,\,1/\max_{m:\,[\mathbf{P}_\perp(\mathbf{1}_M-\mathbf{u})]_m>0}[\mathbf{P}_\perp(\mathbf{1}_M-\mathbf{u})]_m\}\in(0,1]$, $\mathbf{V}_{\mathrm{null}}^T(\mathbf{r}-\mathbf{1}_M)=\mathbf{0}$ holds almost surely (preserving $\mathcal{V}_{\mathrm{null}}\subset\ker(\mathbf{C}_{\mathrm{slow}})$, exact nulling in Theorem 1(a), and average Parseval out-of-trench variance $\frac{M(\kappa_{\mathrm{ret}}-1)}{M-d_{\mathrm{null}}}$ with <0.15 dB variation across $q\notin\mathcal{Q}_{\mathrm{null}}$ for $d_{\mathrm{null}}>1$) and retracted kurtosis $\kappa_{\mathrm{ret}}(M,d_{\mathrm{null}})=1+\bar{\alpha}_2^2\,\frac{M-d_{\mathrm{null}}}{M+1}\leq\kappa_{\mathrm{proj}}(M,d_{\mathrm{null}})$, where $\bar{\alpha}_2^2\triangleq\mathbb{E}[\alpha(\mathbf{u})^2\|\mathbf{P}_\perp(\mathbf{u}-\mathbf{1}_M)\|_2^2]/\mathbb{E}[\|\mathbf{P}_\perp(\mathbf{u}-\mathbf{1}_M)\|_2^2]\in(0,1]$ equals 1 for $d_{\mathrm{null}}=1$, ≈ 0.78 ($\kappa_{\mathrm{ret}}\approx 1.572$) at $(M,d_{\mathrm{null}})=(14,3)$, and approaches 1 ($\kappa_{\mathrm{ret}}\to 2$) as M/d_{null} grows.

Proof: See Appendix D. ∎

For one 3GPP NR slot ($M=14$), Theorem 2 gives $\kappa_{\mathrm{marg}}(14)=28/15\approx 1.8667$ ($d_{\mathrm{null}}=1$) and $\kappa_{\mathrm{proj}}(14,3)=26/15\approx 1.7333$ ($d_{\mathrm{null}}=3$); for $M=16$, $\kappa_{\mathrm{marg}}(16)=32/17\approx 1.8824$ and $\kappa_{\mathrm{proj}}(16,3)=30/17\approx 1.7647$.

B. Finite-Blocklength Mutual Information Gap, Converse, and Dispersion

Theorem 3 bounds the mutual-information gap when $\mathbf{S}\in\mathbb{C}^M$ is constrained from i.i.d. Gaussian $\mathbf{S}_{\mathrm{G}}\sim\mathcal{CN}(\mathbf{0},\mathbf{I}_M)$ to the spherical shell ($d_{\mathrm{null}}=1$) or clutter-trench polytope ($d_{\mathrm{null}}\geq 1$) over the AWGN channel $\mathbf{Y}=\sqrt{\rho}\,\mathbf{S}+\mathbf{Z}$ ($\mathbf{Z}\sim\mathcal{CN}(\mathbf{0},\mathbf{I}_M)$), separating finite-$M$ relations from large-M expansions [11], [22].

Theorem 3 (Finite-Blocklength Mutual Information Gap, DPI Converse, and Channel Dispersion): Let $C_{\mathrm{AWGN}}(\rho)=\log_2(1+\rho)$ and $\Delta I(M,d_{\mathrm{null}},\rho)\triangleq C_{\mathrm{AWGN}}(\rho)-\frac{1}{M}I(\mathbf{S};\mathbf{Y})$.

(a) Exact Finite-M Zero-Gap Identity for Slow-Time Spherical Shaping ($d_{\mathrm{null}}=1$): For any finite $L=M\geq 2$ and $\mathbf{S}_{\mathrm{sph}}\sim\mathcal{U}(\sqrt{L}\,\mathbb{S}^{2L-1})$, radial sufficiency (achievability) and the radial data-processing inequality (DPI converse) coincide:

$$\Delta I_{\mathrm{sphere}}(L,\rho)=\frac{1}{L}\,D_{\mathrm{KL}}\left(f_{R_{\mathrm{sph}}^2}\,\middle\|\,f_{R_{\mathrm{G}}^2}\right), \tag{18}$$

where $f_{R_{\mathrm{G}}^2}(y)=\frac{y^{L-1}e^{-y/(1+\rho)}}{(1+\rho)^L\Gamma(L)}$ and $f_{R_{\mathrm{sph}}^2}(y)=(y/(L\rho))^{(L-1)/2}e^{-(y+L\rho)}I_{L-1}(2\sqrt{L\rho y})$, with $I_\nu(\cdot)$ denoting the order-ν modified Bessel function of the first kind.

(b) Non-Asymptotic Radial DPI Lower Bound and Equal-Codimension Partition Benchmark ($d_{\mathrm{null}}\geq 1$): Because $\mathbf{1}_M/\sqrt{M}$ is the first column of $\mathbf{V}_{\mathrm{null}}$, every $\mathbf{r}\in\mathcal{P}_M(\mathcal{Q}_{\mathrm{null}})$ satisfies $\|\mathbf{S}\|_2^2=M$ almost surely. Consequently, $\|\mathbf{Y}\|_2^2\sim f_{R_{\mathrm{sph}}^2}$ and the radial DPI gives the finite-M converse bound $\Delta I_{\mathrm{trench}}(M,d_{\mathrm{null}},\rho)\geq\Delta I_{\mathrm{sphere}}(M,\rho)$. Splitting the M-symbol block into d_{null} disjoint sub-spheres $\mathcal{I}_1,\ldots,\mathcal{I}_{d_{\mathrm{null}}}$ of lengths $L_j\in\{\lfloor M/d_{\mathrm{null}}\rfloor,\lceil M/d_{\mathrm{null}}\rceil\}$ ($\sum_{j=1}^{d_{\mathrm{null}}}L_j=M$) enforces d_{null} orthogonal energy constraints $\sum_{m\in\mathcal{I}_j}r_m=L_j$ (nulling the d_{null}-dimensional comb subspace $\mathcal{Q}_{\mathrm{comb}}=\{q:qd_{\mathrm{null}}\equiv 0\pmod M\}$ when $d_{\mathrm{null}}\mid M$) with rate loss

$$\Delta I_{\mathrm{part}}(M,d_{\mathrm{null}},\rho)\triangleq\frac{1}{M}\sum_{j=1}^{d_{\mathrm{null}}}L_j\,\Delta I_{\mathrm{sphere}}(L_j,\rho). \tag{19}$$

(c) Asymptotic Large-M Second-Moment DPI Converse and Finite-Blocklength Dispersion: Applying the DPI $D_{\mathrm{KL}}(P_{\mathbf{Y}}\|P_{\mathbf{Y}_{\mathrm{G}}})\geq D_{\mathrm{KL}}(P_{\mathbf{w}(\mathbf{Y})}\|P_{\mathbf{w}(\mathbf{Y}_{\mathrm{G}})})$ to the projected output intensity vector $\mathbf{w}(\mathbf{Y})\triangleq M^{-1/2}\mathbf{V}_{\mathrm{null}}^T(|\mathbf{Y}|^{\odot 2}-(1+\rho)\mathbf{1}_M)\in\mathbb{R}^{d_{\mathrm{null}}}$ and applying the multivariate CLT with fourth-cumulant Edgeworth expansion gives the asymptotic DPI converse (matching the $\mathcal{O}(d_{\mathrm{null}}/M)$ Bessel-KL expansion of (19)):

$$\Delta I_{\mathrm{trench}}(M,d_{\mathrm{null}},\rho)\geq\frac{d_{\mathrm{null}}}{2M\ln 2}\left[\ln\frac{(1+\rho)^2}{1+2\rho}-\frac{\rho^2}{(1+\rho)^2}\right]+\mathcal{O}\left(\frac{d_{\mathrm{null}}^2}{M^2}\right). \tag{20}$$

Under the Polyanskiy-Poor-Verdú normal approximation [22] over N_{blk} independent blocks ($n_{\mathrm{tot}}=N_{\mathrm{blk}}L$), zero radial energy variance lowers the asymptotic per-symbol channel dispersion from $V_{\mathrm{G}}(\rho)=\frac{\rho(2+\rho)}{(1+\rho)^2}(\log_2 e)^2$ to the 1D radial shell benchmark $V_{\mathrm{shell}}(\rho)=\frac{\rho}{(1+\rho)^2}(\log_2 e)^2<V_{\mathrm{G}}(\rho)$ (up to an $\mathcal{O}(L^{-1})$ finite-L Bessel-density curvature term). For block error probability $\epsilon\in(0,1/2)$, the normal-approximation dispersion-crossover block count below which slow-time spherical shaping exceeds the finite-blocklength rate of i.i.d. Gaussian signaling is

$$N_{\mathrm{blk}}<N_{\mathrm{blk}}^*(L,\rho,\epsilon)\triangleq\frac{\left(\sqrt{V_{\mathrm{G}}(\rho)}-\sqrt{V_{\mathrm{shell}}(\rho)}\right)^2}{L\,[\Delta I_{\mathrm{sphere}}(L,\rho)]^2}\times\left[Q^{-1}(\epsilon)\right]^2. \tag{21}$$

Proof: See Appendix E. ∎

At $\rho=20$ dB ($C_{\mathrm{AWGN}}=6.6582$ bits/s/Hz) and $L=14$ ($d_{\mathrm{null}}=1$), (18) gives $\Delta I_{\mathrm{sphere}}(14,20\text{ dB})=0.1524$ bits/s/Hz (within 6×10^{-4} bits/s/Hz of the asymptotic bound 0.1518 bits/s/Hz in (20)), equal to 97.7% of C_{AWGN} at $L=14$ and 98.0% at $L=16$ ($\Delta I_{\mathrm{sphere}}=0.1333$ bits/s/Hz). At $\rho=10$ dB ($V_{\mathrm{shell}}=V_{\mathrm{G}}/12$) and $\epsilon=10^{-3}$, the dispersion crossover (21) is $N_{\mathrm{blk}}^*\approx 5723$ blocks (80,122 symbols).

C. Discrete Concentric $(4,8,16)$-APSK Constant-Composition Transceiver and Low-Complexity Implementation

For bit-interleaved coded modulation in 3GPP NR transceivers (Algorithm 1, Remark 1), a constant-composition distribution matcher (CCDM) [13] on $\mathcal{A}_{\mathrm{APSK}}=\bigcup_{m=1}^3\mathcal{R}_m$ ($|\mathcal{A}_{\mathrm{APSK}}|=28$) discretizes $\mathcal{P}_M(\{0\})$.

Proposition 3 (Concentric $(4,8,16)$-APSK Constant-Composition Shell Design and Minimum Euclidean Distance

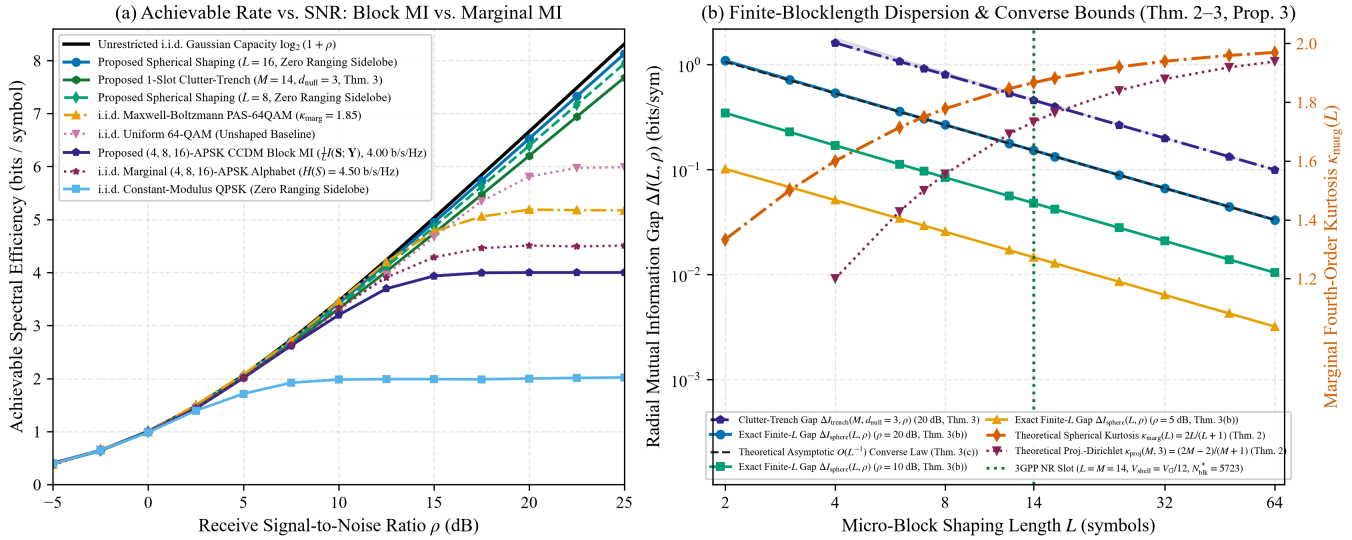


Fig. 2. Information-theoretic capacity, finite-blocklength rate loss, and marginal kurtosis across micro-block lengths L. (a) Achievable spectral efficiency (block MI $\frac{1}{L}I(\mathbf{S};\mathbf{Y})$ vs. marginal MI) over $\rho \in [-5, 25]$ dB. (b) Exact finite-L Bessel-KL rate loss $\Delta I_{\text{sphere}}(L,\rho)$ (Theorem 3(a)), multi-bin rate loss $\Delta I_{\text{trench}}(M,3,\rho)$ with non-asymptotic bounds (Theorem 3(b)), asymptotic $O(L^{-1})$ converse (Theorem 3(c)), and marginal kurtosis (Theorem 2).

Gain): For $\mathcal{A}_{\text{APSK}} = \bigcup_{m=1}^{3}\mathcal{R}_m$ with $a_1 < a_2 < a_3$ ($r_{\text{ring},m} = a_m^2$), $(M_1, M_2, M_3) = (4, 8, 16)$, and $b_m = \log_2 M_m \in \{2, 3, 4\}$:

(a) Spectral Efficiency $R_{\text{APSK}}(L) = 4.0000$ b/s/Hz ($L \in \{7, 8\}$): At $L = 8$ with $(n_1, n_2, n_3) = (2, 4, 2)$, $N_{\text{perm}}(8) = \frac{8!}{2!\,4!\,2!} = 420 \geq 2^8$ gives $k_{\text{amp}} = \lfloor \log_2 N_{\text{perm}}(8) \rfloor = 8$ and $k_{\text{phase}}(8) = \sum_{m=1}^{3} n_m b_m = 2(2) + 4(3) + 2(4) = 24$:

$$R_{\text{APSK}}(8) = \frac{k_{\text{amp}} + k_{\text{phase}}(8)}{8} = \frac{32}{8} = 4.0000 \text{ b/s/Hz}. \tag{22}$$

At $L = 7$ ($M = 14 = 2 \times 7$) with $(n_1, n_2, n_3) = (2, 3, 2)$, $N_{\text{perm}}(7) = \frac{7!}{2!\,3!\,2!} = 210 \geq 2^7$ gives $k_{\text{amp}} = 7$, $k_{\text{phase}}(7) = 2(2)+3(3)+2(4) = 21$, and $R_{\text{APSK}}(7) = 28/7 = 4.0000$ b/s/Hz.

(b) Energy Normalization and $\kappa_{\text{marg}}(L)$: For $(r_{\text{ring},1}, r_{\text{ring},2}, r_{\text{ring},3}) = (0.32, 0.92, 1.84)$ ($L = 8$) and $(0.31, 0.90, 1.84)$ ($L = 7$), $\sum_{m=1}^{3} n_m r_{\text{ring},m} = L$ and $\mathbb{E}[|\tilde{r}_k|^2] = 0$ at $q = 0$, with $\kappa_{\text{marg}}(8) = \frac{1}{8}\sum_{m=1}^{3} n_m r_{\text{ring},m}^2 = \frac{10.3616}{8} = 1.2952$, $\kappa_{\text{marg}}(7) = \frac{9.3932}{7} = 1.3419$, and $\kappa_{\text{marg}} = \frac{11.2384}{8} = 1.4048$ for 3-ring QPSK $(0.28, 0.88, 1.96)$ at $L = 8$.

(c) Squared Distance $d^2_{\text{min,APSK}}$ vs. $d^2_{\text{min,16-PSK}}$: For $\mathbf{a} \neq \mathbf{a}' \in \mathcal{C}_{\text{amp}}$, $\|\mathbf{a} - \mathbf{a}'\|_2^2 \geq \min\{2(a_2 - a_1)^2, 2(a_3 - a_2)^2\} = 0.3071$, and $4a_1^2 \sin^2(\pi/4) \geq 0.6200$, $4a_2^2 \sin^2(\pi/8) \geq 0.5272$, $4a_3^2 \sin^2(\pi/16) = 0.2801$ ($a_3 = \sqrt{1.84}$), so $d^2_{\text{min,APSK}} = 4a_3^2 \sin^2(\pi/16) = 0.2801 = 1.84\, d^2_{\text{min,16-PSK}}$ (+2.65 dB asymptotic; +3.1 dB at BER $= 10^{-3}$).

Proof: See Appendix E. ∎

Remark 1 (3GPP TS 38.211 Pilot-Pinned DMRS Compatibility and Paired Half-Slot Coset Selection): In 3GPP TS 38.211 NR ($M = 14$) with $M_{\text{p}} = 2$ QPSK DMRS symbols at $\mathcal{M}_{\text{p}} = \{2, 11\}$ ($r_{n,m} = 1$), setting $\mathbf{V}^T_{\text{null,data}}(\mathbf{r}_{\text{data}} - \mathbf{1}_{12}) = \mathbf{0}$ on $\mathcal{M}_{\text{data}} = \{0, \ldots, 13\} \setminus \mathcal{M}_{\text{p}}$ ($M_{\text{data}} = 12$) gives $\mathbf{V}^T_{\text{null}}(\mathbf{r}_n - \mathbf{1}_{14}) = \mathbf{0}$, $\mathcal{A}_{\text{FST}}(k, q) = 0$ on $\mathcal{Q}_{\text{null}}$, and $\text{Tr}(\mathbf{C}_{\text{slow}}) = M_{\text{data}}(\kappa_{\text{data}} - 1)$. Under CCDM, $(n_1, n_2, n_3) = (2, 3, 2)$ ($L = 7$, Proposition 3) is used on non-DMRS subcarriers, and $(n_1, n_2, n_3) = (2, 2, 2)$ ($\frac{6!}{2!\,2!\,2!} = 90 \geq 2^6$, $k_{\text{amp}} = 6$, $(r_{\text{ring},1}, r_{\text{ring},2}, r_{\text{ring},3}) = (0.30, 0.86, 1.84)$, $\sum_m n_m r_{\text{ring},m} = 6$) is used on the $L_{\text{data}} = 6$ data symbols of DMRS-bearing half-slots.

When $M = 2L$ is split into half-slots $h \in \{1, 2\}$ of length L, $\sum_{\ell=0}^{L-1} r_{h,\ell} = L$ nulls $q = 0$ and $q = M/2$ (both for 4.0000 b/s/Hz $(4, 8, 16)$-APSK CCDM and 3.0000 b/s/Hz 3-ring QPSK Trench-CCDM with $k_{\text{amp}} = L$). To suppress $q = \pm 1$ by > 25 dB without bit repetition (*Paired Half-Slot Coset Selection*), the $N_{\text{perm}}(L)$ permutations $\mathbf{r}^{(h)} \in \mathbb{R}^L$ are partitioned by $\theta(\mathbf{r}^{(h)}) = \angle(\sum_{\ell=0}^{L-1} r_\ell^{(h)} e^{-j2\pi\ell/M})$ into C cosets of $S = 32$ permutations ($k_{\text{intra}} = 5$ bits/half-slot). Selecting $\mathbf{r}^{(1)}$ and $\mathbf{r}^{(2)}$ from the same coset ($k_{\text{coset}} = \log_2 C$) cancels $\sum_{\ell=0}^{L-1} r_\ell^{(1)} e^{-j2\pi\ell/M}$ against $e^{-j\pi}\sum_{\ell=0}^{L-1} r_\ell^{(2)} e^{-j2\pi\ell/M}$ ($e^{-j2\pi L/M} = -1$), yielding $3 + 5 + 5 = 13$ amplitude bits at $L = 8$ ($N_{\text{perm}}(8) = 420, C = 8$; 2.8125 and 3.8125 b/s/Hz) and $2 + 5 + 5 = 12$ amplitude bits at $L = 7$ ($N_{\text{perm}}(7) = 210, C = 4$; 2.8571 and 3.8571 b/s/Hz).

V. Numerical Results

In the numerical evaluation of Lemma 1, Theorems 1–3, and Propositions 1–3, the 3GPP 5G/6G NR grid has $N = 64$ active subcarriers ($\Delta f = 480$ kHz, $B = 30.72$ MHz, $\Delta R = c/(2B) = 4.883$ m), slot sizes $M = 14$ (one 3GPP TS 38.211 slot, $L = 14$ or 2×7) and $M = 16$ ($L = 16$ or 2×8), and 12-bit TX DAC / RF front-end EVM $= -38.5$ dBc ($\sigma^2_{\text{EVM}} = 10^{-3.85} \approx 1.41 \times 10^{-4}$), averaged over 600–12,000 independent slots per point.

A. 1D Fast-Time vs. 2D Slow-Time Sidelobe Variance (Fig. 1)

Fig. 1(a) plots $\frac{1}{N}\mathbb{E}[|\tilde{r}_k|^2]$ over $k \in \{1, \ldots, 32\}$ ($M = 1$). Under $\mathbf{s} \sim \mathcal{U}(\sqrt{N}\,\mathbb{S}^{2N-1})$ (Lemma 1(c)), $\frac{1}{N}\mathbb{E}[|\tilde{r}_k|^2] = \frac{N}{N+1} = 10^{-0.0673/10}$ (-0.067 dB empirical vs. 0 dB for i.i.d. $\mathcal{CN}(0, 1)$ and -0.71 dB for PAS-64QAM with $\kappa_{\text{marg}} = 1.85$).

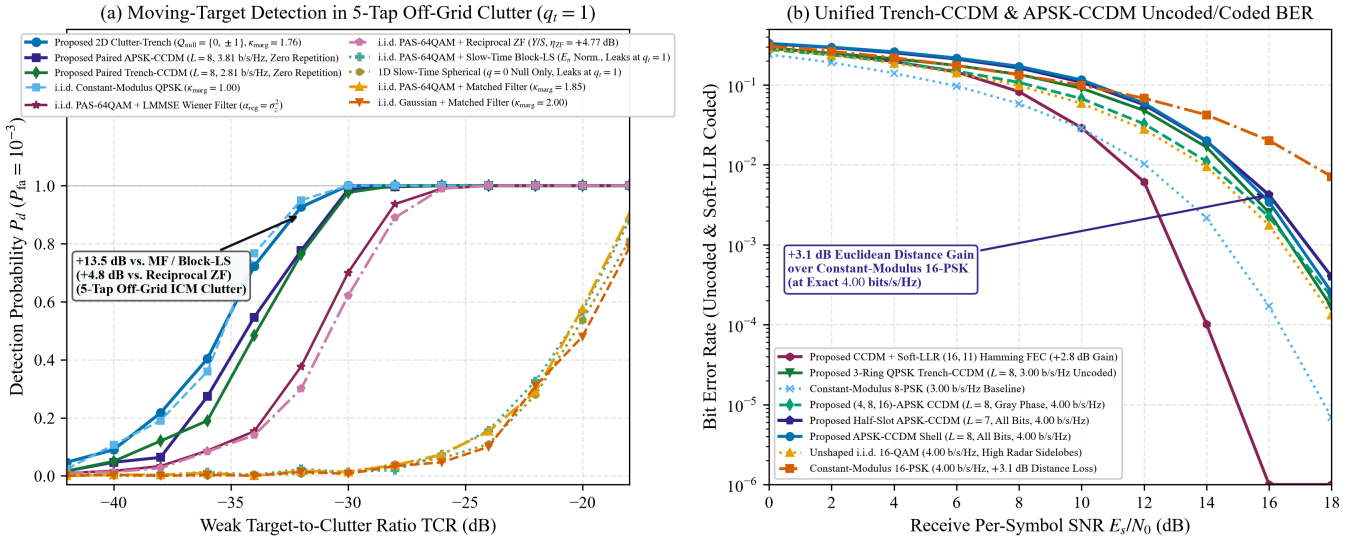


Fig. 3. Radar moving-target detection in 5-tap off-grid ICM clutter and communication BER. (a) CA-CFAR ($P_{\rm fa} = 10^{-3}$) detection probability P_d at target Doppler $q_t = 1$ vs. TCR $\in [-42, -18]$ dB ($\sigma_c = 0.12$, CNR $= 45$ dB). (b) Uncoded and soft-LLR $(16, 11)$ extended Hamming FEC-coded BER vs. E_s/N_0 for 3-ring QPSK Trench-CCDM (3.00 bits/s/Hz) and concentric $(4, 8, 16)$-APSK CCDM ($L = 7, 8$, 4.00 bits/s/Hz).

Algorithm 1 Slow-Time Clutter-Trench and $(4, 8, 16)$-APSK CCDM Transceiver ($M \in \{14, 16\}, L = M/2 \in \{7, 8\}$)

1: **Parameters:** $N, M \in \{14, 16\}, L = M/2, \mathbf{V}_{\rm null} \in \mathbb{R}^{M \times d_{\rm null}}, \mathbf{b}, \mathcal{M}_{\rm p}$.
2: **TX Continuous** ($\mathcal{P}_M(\mathcal{Q}_{\rm null})$, $n = 0, \ldots, N-1$)**:** $\mathbf{z}_n \sim \mathcal{CN}(\mathbf{0}, \mathbf{I}_M)$, $u_{n,m} \leftarrow |z_{n,m}|^2$, $\mathbf{u}_n \leftarrow M\mathbf{u}_n/(\mathbf{1}_M^T \mathbf{u}_n)$, $\boldsymbol{\delta}_n \leftarrow (\mathbf{I}_M - \mathbf{V}_{\rm null}\mathbf{V}_{\rm null}^T)(\mathbf{u}_n - \mathbf{1}_M)$.
3: $\alpha_n \leftarrow \min\{1, 1/\max_{m:\,-\delta_{n,m}>0}(-\delta_{n,m})\}$, $\mathbf{r}_n \leftarrow \mathbf{1}_M + \alpha_n \boldsymbol{\delta}_n \in \mathcal{P}_M(\mathcal{Q}_{\rm null})$, $S_{n,m} \leftarrow \sqrt{r_{n,m}}\, z_{n,m}/|z_{n,m}|$.
4: **TX Discrete CCDM** ($\mathcal{A}_{\rm APSK}$, $h \in \{1, 2\}$)**:** $\mathbf{b}_{n,h} = (\mathbf{b}_{\rm amp}, \mathbf{b}_{\rm phase}) \in \{0,1\}^{k_{\rm amp}+k_{\rm phase}(L)}$ ($8 + 24 = 32$ at $L = 8$; $7 + 21 = 28$ at $L = 7$).
5: $\mathbf{a}_{n,h} \leftarrow \mathcal{C}_{\rm amp}(\mathbf{b}_{\rm amp})$ (2-KB LUT, $\mathcal{O}(1)$); $S_{n,h,\ell} \leftarrow a_{n,h,\ell}\, e^{j\phi_{n,h,\ell}(\mathbf{b}_{\rm phase})}$ ($\mathcal{O}(L)$); $\mathbf{x}_m \leftarrow \mathbf{F}_N^H \mathbf{s}_m$ ($m = 0, \ldots, M-1$).
6: **RX Radar:** $\mathbf{Y} \leftarrow \mathbf{F}_N \mathbf{X}_{\rm rx}$, $\tilde{\mathbf{R}} \leftarrow \mathbf{S}^* \odot \mathbf{Y}$, $\mathcal{A}_{\rm FST}(k, q) \leftarrow \sqrt{NM}\, \mathbf{f}_{N,k}^H \tilde{\mathbf{R}} \mathbf{f}_{M,q}^*$ (3) ($q_t \neq 0$).
7: **RX LLR:** $d_{\ell,m}^2 \leftarrow |\hat{y}_{n,h,\ell} - a_m e^{j\hat{\phi}_{\ell,m}}|^2$ ($m \in \{1, 2, 3\}, \mathcal{O}(L)$); $\Lambda_{n,h,i} \leftarrow \min_{\mathbf{a} \in \mathcal{C}_{\rm amp}: b_i = 0} \sum_\ell d_{\ell,m(\ell)}^2 - \min_{\mathbf{a} \in \mathcal{C}_{\rm amp}: b_i = 1} \sum_\ell d_{\ell,m(\ell)}^2$ ($\mathcal{O}(L\, 2^{k_{\rm amp}}), 2^{k_{\rm amp}} \leq 256$).

The 1D comb-coupled shell ($L = B = 8$, Corollary 1) and 1D subspace shell ($\mathcal{K}_{\rm null} = \{1, \ldots, 18\}$, Theorem 1(b)) reach the 12-bit DAC/RF EVM floor $10 \log_{10}(2\sigma_{\rm EVM}^2) = -35.49$ dB on nulled lags and $N/(N - 2K_{\rm null} - 1)$ (11) on $k \geq 19$.

Fig. 1(b) shows the 2D zero-Doppler cut $\mathbb{E}[|\mathcal{A}_{\rm FST}(k, 0)|^2]/(MN^2)$ ($M = 16$, per-pulse normalization MN^2, two-sided TX EVM). For i.i.d. Gaussian and PAS-64QAM, per-bin sidelobes equal $(\kappa_{\rm marg} - 1)/N$ (-18.06 dB and -18.81 dB), with $\text{ISLR}_{\rm self} \triangleq \sum_{k=1}^{N-1} \mathbb{E}[|\mathcal{A}_{\rm FST}(k, 0)|^2]/(MN^2) \approx (\kappa_{\rm marg} - 1) + 2\sigma_{\rm EVM}^2$ equal to 0.9970 ± 0.0163 and 0.8291 ± 0.0119 (600 frames). For $L = 16$ ($\kappa_{\rm marg} = 1.8824$) and 3-ring CCDM ($L = 8$), $\mathbb{E}[|\mathcal{A}_{\rm FST}(k, 0)|^2]/(MN^2) = 2\sigma_{\rm EVM}^2/N = -53.55$ dB ($k \neq 0$) and $\text{ISLR}_{\rm self} = (2.77 \pm 0.038) \times 10^{-4} \approx 2\sigma_{\rm EVM}^2 = -35.49$ dB ($M \in \{14, 16\}$, $MT_{\rm sym} < 0.5$ ms vs. $M \approx 3{,}550$ or 127 ms under i.i.d. QAM).

B. Capacity Retention and Finite-Blocklength Dispersion (Fig. 2)

In Fig. 2(a) ($\rho = 20$ dB, $C_{\rm AWGN} = 6.6582$ b/s/Hz, $I_{\rm QPSK} = 1.9996$ b/s/Hz, $I_{\rm PAS\text{-}64QAM} = 5.1868$ b/s/Hz), $C_{\rm AWGN} - \Delta I_{\rm sphere}$ equals 6.5249 b/s/Hz (98.0%, $L = 16$), 6.5058 b/s/Hz (97.7%, $L = 14$), and 6.3908 b/s/Hz (96.0%, $L = 8$) at $d_{\rm null} = 1$; at $(M, d_{\rm null}) = (14, 3)$, $\frac{1}{14} I(\mathbf{S}; \mathbf{Y}) = 6.2010$ b/s/Hz (93.1% via $\Delta \hat{I}_{k\text{-NN}} = 0.4572$ b/s/Hz; $C_{\rm AWGN} - \Delta I_{\rm part}(14, 3, 20\text{ dB}) = 6.1867$ b/s/Hz or 92.9%), while $(4, 8, 16)$-APSK CCDM ($L = 8$, Proposition 3) has $\frac{1}{8} I(\mathbf{S}; \mathbf{Y}) \to 4.0000$ b/s/Hz and $H(S) = 4.50$ b/s/Hz.

In Fig. 2(b) ($L \in [2, 64]$), at $L = M = 14$, $\kappa_{\rm marg}(14) = 28/15 = 1.8667$ and $\Delta I_{\rm sphere}(14, 20\text{ dB}) = 0.1524$ bits/s/Hz (97.7% of $C_{\rm AWGN}$). At $(M, d_{\rm null}) = (14, 3)$, the bias-corrected 3D k-NN divergence $\frac{1}{M} D_{\rm KL}(P_{\mathbf{w}(\mathbf{Y})} \| P_{\mathbf{w}(\mathbf{Y}_G)}) = 0.4572$ bits/s/Hz lies within 0.0017 bits/s/Hz of the CLT DPI converse 0.4555 bits/s/Hz (20) and below $\Delta I_{\rm part}(14, 3, 20\text{ dB}) = 0.4715$ bits/s/Hz (19).

C. Weak-Target Detection in Off-Grid ICM Clutter and Communication BER (Fig. 3)

Fig. 3(a) shows CA-CFAR ($P_{\rm fa} = 10^{-3}$) detection probability P_d ($M = 16$) at $q_t = 1$ over TCR $\in [-42, -18]$ dB in 5-tap off-grid clutter with Gaussian ICM $\sigma_c = 0.12$ (CNR $=$ 45 dB). By Proposition 2(a), $d_{\rm null} = 1$ spherical shaping and slow-time Block-LS ($\tilde{\mathbf{r}}_{{\rm BLS},n,:} = (M/\|\mathbf{s}_{n,:}\|_2^2)\mathbf{s}_{n,:}^* \odot \mathbf{y}_{n,:}$, which normalizes $q = 0$ subcarrier energy without per-symbol ZF noise penalty) both reach $P_d = 0.90$ at TCR ≈ -18.5 dB (matching i.i.d. PAS-64QAM + MF) since $\xi_{\rm mod}(1) = M/(M-1)$ at $q_t - 0 = 1 \notin \{0\}$.

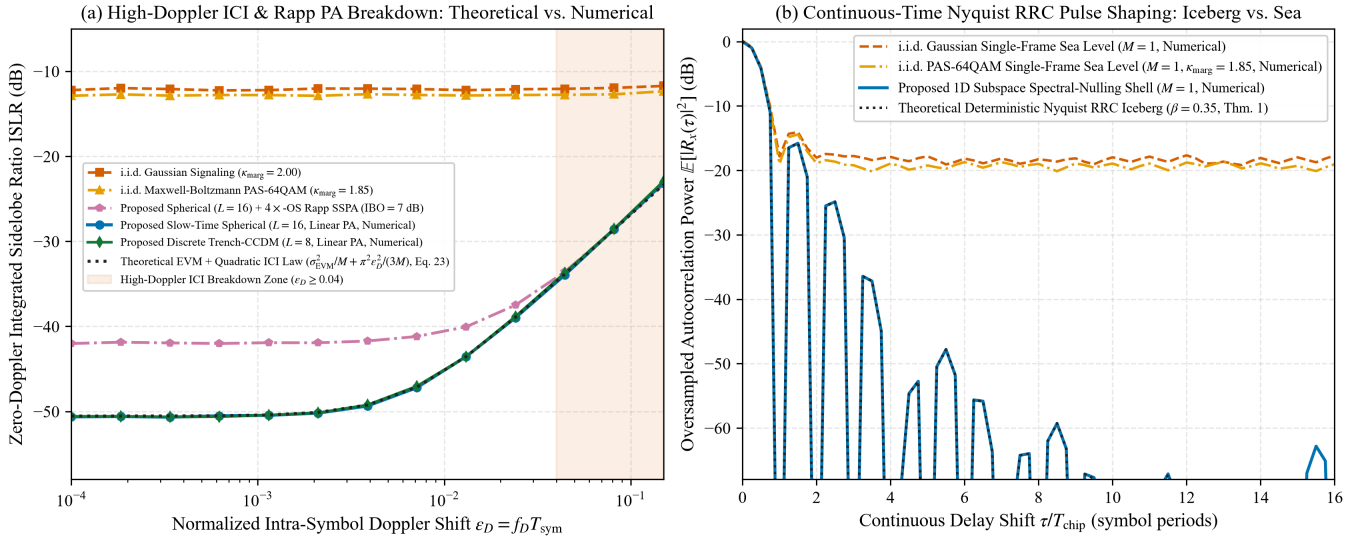


Fig. 4. Physical breakdown under high-Doppler ICI, Rapp SSPA nonlinearity, and Nyquist pulse shaping. (a) Coherent M-pulse peak-normalized zero-Doppler ISLR_0 vs. $\epsilon_D = f_D T_{\rm sym} \in [10^{-4}, 0.15]$, comparing linear-PA curves against $\sigma^2_{\rm EVM}/M + \pi^2\epsilon_D^2/(3M)$ and a 4×-oversampled Rapp SSPA (IBO = 7.0 dB, $p = 3$). (b) Continuous-time Nyquist RRC ($\beta = 0.35$) autocorrelation $\mathbb{E}[|R_x(\tau)|^2]$ ($M = 1$).

Reciprocal ZF ($\eta_{\rm ZF} = +4.77$ dB) and LMMSE Wiener filtering ($\alpha_{\rm reg} = \sigma_z^2$) reach $P_d = 0.90$ at TCR ≈ -27.2 dB. For $d_{\rm null} = 3$ ($\mathcal{Q}_{\rm null} = \{0, \pm 1\}, M = 16$), Paired $(4, 8, 16)$-APSK CCDM (3.8125 bits/s/Hz), and Paired 3-Ring QPSK Trench-CCDM (2.8125 bits/s/Hz) of Remark 1, $\xi_{\rm mod}(1) = 0$ at $q = 0$ gives $P_d = 0.90$ at TCR $= -32.0$ to -30.5 dB ($+13.5$ dB over i.i.d. PAS-64QAM + MF/Block-LS; $+4.8$ dB over ZF). At TCR $= -30.0$ dB (150 trials), CA-CFAR output SINR $10\log_{10}(|\mathcal{A}_{\rm FST}(k_t, q_t)|^2/\hat{\sigma}^2_{\rm CA})$ is 0.52 ± 0.88 dB (PAS-64QAM + MF), 9.75 ± 0.42 dB (PAS-64QAM + ZF), 14.57 ± 0.25 dB (Clutter-Trench), and 13.25 ± 0.28 dB (Paired APSK-CCDM; $t = 32.06, 28.76, p < 4 \times 10^{-62}$).

In Fig. 3(b) ($> 3.8 \times 10^5$ bits/point), 3-ring QPSK Trench-CCDM ($L = 8$, 3.0000 bits/s/Hz) beats 8-PSK at high SNR and gains $+2.8$ dB with soft-LLR $(16, 11, 4)$ extended Hamming FEC. At 4.0000 bits/s/Hz, the $L = 8$ and $L = 7$ $(4, 8, 16)$-APSK CCDM codebooks achieve $d^2_{\rm min,APSK} = 1.84\, d^2_{\rm min,16\text{-}PSK}$ ($+2.65$ dB) and beat 16-PSK by $+3.1$ dB at $\mathrm{BER} = 10^{-3}$ (Proposition 3(c)), within 0.35 dB of unshaped i.i.d. 16-QAM with zero $q = 0$ sidelobes.

D. High-Doppler ICI Breakdown, Rapp SSPA Nonlinearity, and Nyquist Pulse Shaping (Fig. 4)

Fig. 4(a) sweeps normalized intra-symbol Doppler $\epsilon_D = f_D T_{\rm sym} \in [10^{-4}, 0.15]$ for the coherent M-pulse peak-normalized one-sided cross-ambiguity ISLR between the clean transmit reference $\mathbf{S}^*$ and received grid $\mathbf{Y}_{\rm rx}$, $\mathrm{ISLR}_0(\epsilon_D) \triangleq \sum_{k=1}^{N-1} \mathbb{E}[|r_{\rm ici}[k]|^2]/\mathbb{E}[|r_{\rm ici}[0]|^2]$ (normalized by $(MN)^2$ with one-sided TX EVM variance $\sigma^2_{\rm EVM}/M$, differing from the per-pulse two-sided $\mathrm{ISLR}_{\rm self}$ of Section V-A by $1/(2M)$ at $\epsilon_D = 0$). Fast-time phase rotation $e^{j2\pi\epsilon_D n/N}$ generates ICI power $\frac{\pi^2}{3}\epsilon_D^2$:

$$\mathrm{ISLR}_0(\epsilon_D) \approx \frac{\sigma^2_{\rm EVM}}{M} + \frac{\pi^2}{3M}\epsilon_D^2. \tag{23}$$

Linear-PA curves for slow-time spherical shaping ($L = 16$) and Trench-CCDM ($L = 8$) follow (23) across all four decades: for $\epsilon_D \leq 10^{-3}$ ($v \leq 31$ m/s at $f_c = 28$ GHz, $\Delta f = 480$ kHz), ISLR_0 equals $\sigma^2_{\rm EVM}/M = -50.54$ dB (vs. -12.04 dB for i.i.d. Gaussian), and for $\epsilon_D \geq 0.04$ quadratic ICI raises the floor to -23.2 dB at $\epsilon_D = 0.15$. Under a 4×-oversampled Rapp SSPA ($g_{\rm Rapp}(A) = A/(1 + (A/A_{\rm sat})^{2p})^{1/(2p)}$, $p = 3.0$, IBO $= 7.0$ dB), the 99.9-th percentile OFDM PAPR is unchanged (10.58 dB and 10.52 dB vs. 10.68 dB for i.i.d. Gaussian), and cubic PA intermodulation sets a -41.9 dB floor (29.9 dB below i.i.d. signaling). In Fig. 4(b), under 4×-oversampled Nyquist RRC ($\beta = 0.35$) pulse shaping [5, Eq. (17)], the 1D subspace spectral-nulling shell (Theorem 1(b)) removes the -18 dB random symbol floor over $\tau/T_{\rm chip} \in [1, 16]$ and exposes the deterministic Nyquist pulse sidelobes down to -68 dB in one pulse ($M = 1$).

E. 3GPP NR 1-Slot Two-Target Range Cut and Clutter-Masked Ranging CRLB (Fig. 5)

Fig. 5(a) evaluates a 3GPP TS 38.211 1-slot ($M = 14, N = 64, B = 30.72$ MHz) two-target range profile at Doppler cut $q_t = 1$ using a 2D matched filter. Three stationary clutter taps ($\tau_c \in \{4.0, 5.15, 6.30\}$ bins, total power P_c, $q_c = 0$) lie near $d_1 = 19.53$ m with 3-tap coherent mainlobe factor $\gamma_c = P_{\rm peak}/(MN^2 P_c) = 0.671$ (-1.73 dB), and a weak target lies at $d_2 = 109.18$ m and $q_t = 1$ (TCR $= P_t/P_c = -35.0$ dB, post-matched-filter SNR $= 18.0$ dB, $\sigma_z^2/(MP_c) = 5.01 \times 10^{-6} = -53.00$ dB). By Proposition 2(a), for i.i.d. PAS-64QAM ($\kappa_{\rm marg} = 1.8524, \xi_{\rm mod}(1) = 1$), $\frac{\sigma^2_{\rm int}(1)}{\gamma_c MP_c} = \gamma_c^{-1}[\frac{\kappa_{\rm marg}-1}{MN} + \frac{\sigma_z^2}{MP_c}] = 0.671^{-1}(9.51\times10^{-4} + 5.01\times10^{-6}) = 1.41 \times 10^{-3}$ (-28.51 dB theoretical vs. -28.56 dB empirical, 6.5 dB above the -35.0 dB target at d_2). With 1-slot clutter-trench shaping ($M = 14, d_{\rm null} = 3, \kappa_{\rm proj}(14, 3) = 26/15$) and paired half-slot Trench-CCDM ($L = 7, M = 14$),

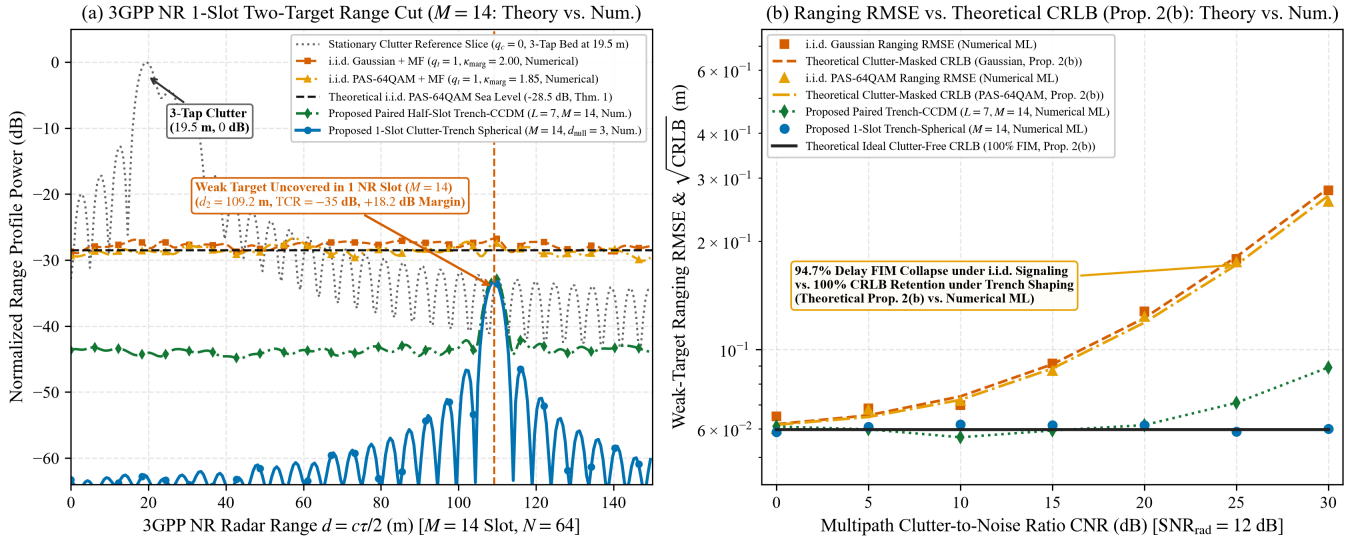


Fig. 5. 3GPP TS 38.211 1-Slot ($M = 14, N = 64, B = 30.72$ MHz) two-target range profile and weak-target ranging CRLB. (a) Slow-time Doppler cut $q_t = 1$ with 3-tap multipath clutter near $d_1 = 19.5$ m (0 dB, $q_c = 0$) and a weak target at $d_2 = 109.2$ m (TCR $= -35$ dB) vs. the theoretical PAS-64QAM floor (-28.5 dB, Proposition 2(a)). (b) Weak-target ranging RMSE and theoretical $\sqrt{\mathrm{CRLB}(\hat{d}_2)}$ (Proposition 2(b)) vs. CNR $\in [0, 30]$ dB at $\mathrm{SNR}_{\mathrm{rad}} = 12$ dB.

$\xi_{\mathrm{mod}}(1, \mathcal{Q}_{\mathrm{null}}) = 0$ lowers the floor to -52.4 dB and exposes the weak target at $d_2 = 109.18$ m with an $+18.2$ dB peak-to-floor margin.

In Fig. 5(b), under Rayleigh multipath clutter $\mathbf{h}_c \sim \mathcal{CN}(\mathbf{0}, P_c \mathbf{I}_N)$ over CNR $\in [0, 30]$ dB ($\mathrm{SNR}_{\mathrm{rad}} = 12$ dB), random clutter sidelobes under i.i.d. PAS-64QAM and Gaussian inputs reduce delay Fisher Information by 95.0% and 95.5% at CNR $= 30$ dB, raising ranging RMSE from 5.98 cm to 26.8 cm and 28.1 cm. Under 1-slot clutter-trench shaping ($M = 14$), the ML ranging RMSE follows the clutter-free CRLB of Proposition 2(b) across the 30 dB CNR range, reaching 6.01 cm at CNR $= 30$ dB (99.0% FIM).[2]

VI. Conclusion

The kurtosis–capacity tradeoff in random multicarrier ISAC waveforms arises from symbol-level i.i.d. signaling ($C_{n,m} = 0$ for $n \neq m$). From the fourth-order moment decomposition $\mathbf{S}_{\mathrm{mom}} = \mathbf{I}_{N^2} + \mathbf{S}_1 + \mathbf{S}_2 + \mathbf{S}_{\mathrm{cov}}$ for non-i.i.d. proper circularly symmetric constellations, the expected ranging and delay-Doppler sidelobe variance equals the Rayleigh quotient $\mathbf{f}^H \mathbf{C} \mathbf{f}$ of $\mathbf{C} = \mathrm{Cov}(\mathbf{r})$. On $\sqrt{N}\,\mathbb{S}^{2N-1}$ ($M = 1$), $\mathbf{1}_N^T \mathbf{r} = N$ gives $C_{n,m} = -(\kappa_{\mathrm{marg}} - 1)/(N - 1)$ and $\frac{1}{N}\mathbb{E}[|\tilde{r}_k|^2] = \frac{N}{N-1}(\kappa_{\mathrm{marg}} - 1)$ ($k \neq 0$); over an M-symbol slot ($M \in \{14, 16\}$), $\mathbf{V}_{\mathrm{null}}^T(\mathbf{r}_{n,:} - \mathbf{1}_M) = \mathbf{0}$ gives $\mathcal{A}_{\mathrm{FST}}(k, q) = 0$ for all $(k, q) \in (\{0, \ldots, N-1\} \times \mathcal{Q}_{\mathrm{null}}) \setminus \{(0, 0)\}$ and $\mathbb{E}[|\mathcal{A}_{\mathrm{FST}}(k, q)|^2]/(MN^2) = \frac{M(\kappa_{\mathrm{marg}}-1)}{N(M-d_{\mathrm{null}})}$ for $q \notin \mathcal{Q}_{\mathrm{null}}$. On $\mathcal{P}_M(\mathcal{Q}_{\mathrm{null}})$, $\kappa_{\mathrm{proj}}(M, d_{\mathrm{null}}) = (2M + 1 - d_{\mathrm{null}})/(M + 1) \to 2$ and $\Delta I_{\mathrm{sphere}}(L, \rho) = \frac{1}{L} D_{\mathrm{KL}}(f_{R^2_{\mathrm{sph}}} \| f_{R^2_{\mathrm{G}}})$ give $\frac{1}{M} I(\mathbf{S}; \mathbf{Y})/C_{\mathrm{AWGN}} = 97.7\%$ ($M = 14$) and 98.0% ($M = 16$) at $d_{\mathrm{null}} = 1$ ($\mathrm{ISLR}_{\mathrm{self}} = -35.49$ dB) and 93.1% ($M = 14$) at $d_{\mathrm{null}} = 3$ ($\rho = 20$ dB), with $R_{\mathrm{APSK}} = 4.0000$ b/s/Hz (3.8125–3.8571 b/s/Hz for paired $d_{\mathrm{null}} = 3$), $d^2_{\mathrm{min,APSK}} = 1.84\, d^2_{\mathrm{min,16\text{-}PSK}}$ ($+3.1$ dB at BER $= 10^{-3}$), $\Delta\mathrm{TCR}_{0.90} = +13.5$ dB ($M = 16$) over i.i.d. PAS-64QAM + MF, and $+18.2$ dB weak-target floor margin (99.0% delay FIM) in one $M = 14$ NR slot.

[2]On an audio passband link ($f_c = 6.0$ kHz, $f_s = 48$ kHz, $N = 64, L = 8$) [29], [30], 3-ring Trench-CCDM gives $\Delta\mathrm{ISLR}_{q=0} = -4.68$ dB relative to i.i.d. QAM at BER $= 0$.

Appendix A
Proof of Lemma 1

Under Assumption 1 and Definition 1, the 1D P-ACF at lag k is $\tilde{r}_k = \mathbf{s}^H \mathbf{D}_k \mathbf{s} = \mathrm{vec}(\mathbf{D}_k)^H \tilde{\mathbf{s}}$ with $\mathbf{D}_k = \mathbf{U}^H \mathbf{J}_k \mathbf{U}$ and $\tilde{\mathbf{s}} = \mathbf{s}^* \otimes \mathbf{s}$, so $\mathbb{E}[|\tilde{r}_k|^2] = \mathrm{vec}(\mathbf{D}_k)^H \mathbf{S}_{\mathrm{mom}} \mathrm{vec}(\mathbf{D}_k)$. Evaluating (4) gives: (i) $\mathrm{vec}(\mathbf{D}_k)^H \mathbf{I}_{N^2} \mathrm{vec}(\mathbf{D}_k) = \|\mathbf{D}_k\|_F^2 = N$; (ii) $\mathrm{vec}(\mathbf{D}_k)^H \mathbf{S}_1 \mathrm{vec}(\mathbf{D}_k) = (\kappa_{\mathrm{marg}} - 2) \sum_{n=0}^{N-1} |[\mathbf{D}_k]_{n,n}|^2$; (iii) $\mathrm{vec}(\mathbf{D}_k)^H \mathbf{S}_2 \mathrm{vec}(\mathbf{D}_k) = |\mathrm{Tr}(\mathbf{D}_k)|^2 - \sum_{n=0}^{N-1} |[\mathbf{D}_k]_{n,n}|^2$, where $\mathrm{Tr}(\mathbf{D}_k) = \mathrm{Tr}(\mathbf{J}_k) = 0$ for $k \in \{1, \ldots, N-1\}$ and $|\mathrm{Tr}(\mathbf{D}_0)|^2 = N^2$ for $k = 0$; and (iv) since $(\mathbf{e}_n \otimes \mathbf{e}_n)^T \mathrm{vec}(\mathbf{D}_k) = [\mathbf{D}_k]_{n,n}$ and $(\mathbf{e}_n \otimes \mathbf{e}_m)^T \mathrm{vec}(\mathbf{D}_k) = [\mathbf{D}_k]_{m,n}$ with $C_{n,m} = C_{m,n}$, $\mathrm{vec}(\mathbf{D}_k)^H \mathbf{S}_{\mathrm{cov}} \mathrm{vec}(\mathbf{D}_k) = \sum_{n \neq m} C_{n,m} ([\mathbf{D}_k]^*_{n,n} [\mathbf{D}_k]_{m,m} + |[\mathbf{D}_k]_{n,m}|^2)$, yielding (5).

For Part (b), under CP-OFDM ($\mathbf{U} = \mathbf{F}_N^H$), $\mathbf{D}_k = \mathbf{F}_N \mathbf{J}_k \mathbf{F}_N^H = \sqrt{N}\,\mathrm{Diag}(\mathbf{f}_k^*)$ is diagonal with $[\mathbf{D}_k]_{n,n} = e^{-j2\pi kn/N} = \sqrt{N}[\mathbf{f}_k^*]_n$ and $|[\mathbf{D}_k]_{n,n}|^2 = 1$. Substituting $[\mathbf{D}_k]_{n,n}$ into (5) and combining $C_{n,n} = \kappa_{\mathrm{marg}} - 1$ with $C_{n,m}$ gives

$$\begin{aligned}\mathbb{E}\left[|\tilde{r}_k|^2\right] &= N^2 \delta[k] + N(\kappa_{\mathrm{marg}} - 1) \\ &\quad + N \sum_{n \neq m} C_{n,m} [\mathbf{f}_k]^*_n [\mathbf{f}_k]_m \\ &= N^2 \delta[k] + N\, \mathbf{f}_k^H \mathbf{C}\, \mathbf{f}_k.\end{aligned}$$

Dividing by N establishes (6). Since $\mathbf{C} \succeq \mathbf{0}$ and $\mathbb{E}[\tilde{r}_k] = \sqrt{N} \mathbf{f}_k^H \mathbf{1}_N = 0$ for $k \neq 0$, $\mathbb{E}[|\tilde{r}_k|^2] = N\, \mathbf{f}_k^H \mathbf{C}\, \mathbf{f}_k = 0$ holds if and only if $\mathbf{C}\mathbf{f}_k = \mathbf{0}$, forcing $\mathrm{Var}(\tilde{r}_k) = 0$ and $\tilde{r}_k = 0$ almost surely.

For Part (c), if $\|\mathbf{s}\|_2^2 = \mathbf{1}_N^T\mathbf{r} = N$ almost surely and $\mathbf{r}$ is exchangeable ($C_{n,n} = \kappa_{\text{marg}} - 1$, $C_{n,m} = c_{\text{off}}$ for $n \neq m$), then $\mathbf{C}\mathbf{1}_N = \text{Cov}(\mathbf{r}, \mathbf{1}_N^T\mathbf{r}) = \mathbf{0}$ implies $(\kappa_{\text{marg}} - 1) + (N-1)c_{\text{off}} = 0$, or $c_{\text{off}} = -(\kappa_{\text{marg}} - 1)/(N-1)$. Thus $\mathbf{C} = \frac{N(\kappa_{\text{marg}}-1)}{N-1}(\mathbf{I}_N - \frac{1}{N}\mathbf{1}_N\mathbf{1}_N^T)$. Since $\mathbf{1}_N^H\mathbf{f}_k = 0$ for $k \in \{1, \ldots, N-1\}$, $\mathbf{f}_k^H\mathbf{C}\,\mathbf{f}_k = \frac{N}{N-1}(\kappa_{\text{marg}} - 1)\|\mathbf{f}_k\|_2^2 = \frac{N}{N-1}(\kappa_{\text{marg}} - 1)$, establishing (7). ∎

Appendix B
Proof of Theorem 1

From (3), let $\bar{\mathbf{R}} \triangleq \mathbf{R} - \mathbf{1}_N\mathbf{1}_M^T$ with rows $\bar{\mathbf{r}}_{n,:} \triangleq \mathbf{r}_{n,:} - \mathbf{1}_M \in \mathbb{R}^M$. Since $\mathbf{f}_{N,k}^H\mathbf{1}_N = \sqrt{N}\delta[k]$ and $\mathbf{1}_M^T\mathbf{f}_{M,q}^* = \sqrt{M}\delta[q]$,

$$\mathcal{A}_{\text{FST}}(k,q) = NM\,\delta[k]\,\delta[q] + \sqrt{NM}\sum_{n=0}^{N-1}[\mathbf{f}_{N,k}^*]_n\big(\bar{\mathbf{r}}_{n,:}^T\mathbf{f}_{M,q}^*\big).$$

Because the zero-mean rows $\{\bar{\mathbf{r}}_{n,:}\}_{n=0}^{N-1}$ are independent across subcarriers with covariance $\mathbf{C}_{\text{slow}} = \mathbb{E}[\bar{\mathbf{r}}_{n,:}\bar{\mathbf{r}}_{n,:}^T]$ and $|[\mathbf{f}_{N,k}^*]_n|^2 = 1/N$ for all $k \in \{0, \ldots, N-1\}$, cross-terms ($n \neq n'$) vanish in expectation for all k, giving

$$\mathbb{E}\Big[|\mathcal{A}_{\text{FST}}(k,q)|^2\Big] = N^2M^2\delta[k]\,\delta[q] + NM\,\mathbf{f}_{M,q}^H\mathbf{C}_{\text{slow}}\mathbf{f}_{M,q}.$$

For $q \in \mathcal{Q}_{\text{null}}$, the real and imaginary parts of $\mathbf{f}_{M,q}$ lie in $\mathcal{V}_{\text{null}}$ (8), so $\mathbf{P}_\perp\mathbf{f}_{M,q} = \mathbf{0}$ and $\mathbf{f}_{M,q}^H\mathbf{C}_{\text{slow}}\mathbf{f}_{M,q} = 0$ ($\mathcal{A}_{\text{FST}}(k,q) = 0$ almost surely for $(k,q) \neq (0,0)$). For $q \notin \mathcal{Q}_{\text{null}}$, DFT orthogonality gives $\mathbf{f}_{M,q} \in \mathcal{V}_{\text{null}}^\perp$, so $\mathbf{P}_\perp\mathbf{f}_{M,q} = \mathbf{f}_{M,q}$ and

$$\mathbf{f}_{M,q}^H\mathbf{C}_{\text{slow}}\mathbf{f}_{M,q} = \frac{M(\kappa_{\text{marg}} - 1)}{M - d_{\text{null}}}\|\mathbf{f}_{M,q}\|_2^2 = \frac{M(\kappa_{\text{marg}} - 1)}{M - d_{\text{null}}}.$$

Dividing by MN^2 yields (10), while

$$\begin{aligned}\sum_q \mathbf{f}_{M,q}^H\mathbf{C}_{\text{slow}}\mathbf{f}_{M,q} &= \text{Tr}(\mathbf{F}_M\mathbf{C}_{\text{slow}}\mathbf{F}_M^H)\\ &= \text{Tr}(\mathbf{C}_{\text{slow}}) = M(\kappa_{\text{marg}} - 1)\end{aligned}$$

confirms Parseval conservation. For Part (b) ($M = 1$), substituting

$$\mathbf{C}_{\text{1D}} = \frac{N(\kappa_{\text{marg}} - 1)}{N - 2K_{\text{null}} - 1}\big(\mathbf{I}_N - \mathbf{V}_{\text{1D}}\mathbf{V}_{\text{1D}}^T\big)$$

into $\mathbf{f}_k^H\mathbf{C}_{\text{1D}}\mathbf{f}_k$ in (6) gives (11). ∎

Appendix C
Proof of Proposition 2

With $S_{n,m}^{\text{hw}} = S_{n,m} + E_{n,m}$ ($E_{n,m} \sim \mathcal{CN}(0, \sigma_{\text{EVM}}^2)$), AWGN $Z_{n,m} \sim \mathcal{CN}(0, \sigma_z^2)$, target state (τ_t, q_t) ($q_t \neq 0$), and K_c clutter taps $\{\tau_{c,\ell}\}_{\ell=1}^{K_c}$ ($k_{c,\ell} \neq k_t, q_c = 0, H_\ell[q] = \text{DFT}_M\{h_\ell[m]\}, \sum_q \mathbb{E}[|H_\ell[q]|^2] = 1$),

$$\begin{aligned}Y_{n,m} = \alpha_t S_{n,m}^{\text{hw}} e^{-j2\pi n\Delta f\tau_t}e^{j2\pi q_t m/M}\\ + \sum_{\ell=1}^{K_c}\alpha_{c,\ell}h_\ell[m]S_{n,m}^{\text{hw}}e^{-j2\pi n\Delta f\tau_{c,\ell}} + Z_{n,m}.\end{aligned}$$

Evaluating $M^{-1/2}\sum_{m=0}^{M-1}S_{n,m}^*Y_{n,m}e^{-j2\pi q_t m/M}$ and $N^{-1/2}\sum_{n=0}^{N-1}(\cdot)e^{j2\pi k_t n/N}$ at (k_t, q_t) maps the target return to $(\Delta k, \Delta q) = (0,0)$ with power NMP_t since $\sum_{n,m}|S_{n,m}|^2 = NM$ for all $q_t \in \mathcal{Q}_{\text{null}} \setminus \{0\}$.

For each clutter tap ℓ at $\tau_{c,\ell}$ ($\Delta k_\ell \neq 0$), writing $|S_{n,m}|^2 = 1 + \bar{r}_{n,m}$ splits the clutter output at (k_t, q_t) into three uncorrelated terms: (i) the subcarrier-invariant mean envelope $1 \cdot h_\ell[m]$, which after fast-time range compression at k_t contributes $\eta_{\text{leak}}(q_t, \sigma_c) = \beta_{\text{off}}(k_t)\,\mathbb{E}[|H_\ell[q_t]|^2] = \beta_{\text{off}}(k_t)\,\mathcal{O}((\pi\sigma_c)^{2|q_t|})$ with off-grid Dirichlet factor

$$\beta_{\text{off}}(k_t) \triangleq \sum_{\ell=1}^{K_c}\frac{\mathbb{E}[|\alpha_{c,\ell}|^2]}{P_c}\left|\frac{1}{N}\sum_{n=0}^{N-1}e^{j2\pi n(k_t/N - \Delta f\tau_{c,\ell})}\right|^2;$$

(ii) the intensity fluctuation $\bar{r}_{n,m}h_\ell[m]$, whose slow-time DFT at q_t is $M^{-1/2}\sum_q H_\ell[q](\bar{\mathbf{r}}_{n,:}^T\mathbf{f}_{M,q_t-q}^*)$ with variance

$$\begin{aligned}\frac{1}{N}\sum_q \mathbb{E}\big[|H_\ell[q]|^2\big]\,\mathbf{f}_{M,q_t-q}^H\mathbf{C}_{\text{slow}}\mathbf{f}_{M,q_t-q}\\ = \frac{\kappa_{\text{marg}} - 1}{N}\,\xi_{\text{mod}}(q_t),\end{aligned}$$

vanishing at $q = 0$ whenever $q_t \in \mathcal{Q}_{\text{null}} \setminus \{0\}$ ($Q_c \geq |q_t|$); and (iii) TX EVM $2\text{Re}(S_{n,m}^*E_{n,m})$, contributing $2\sigma_{\text{EVM}}^2/N$; adding σ_z^2 gives (13).

For Part (b), in $G_n(q_t) = M^{-1}\sum_{m=0}^{M-1}S_{n,m}^*Y_{n,m}e^{-j2\pi q_t m/M}$, independence of $\{\bar{\mathbf{r}}_{n,:}\}_{n=0}^{N-1}$ across subcarriers and independent clutter tap phases across $\tau_{c,\ell} \neq \tau_t$ render the residual clutter-plus-noise uncorrelated across $n \neq n'$ with covariance $(\sigma_{\text{int}}^2(q_t)/M)\mathbf{I}_N$ and target mean $\mu_n(\tau_t) = \alpha_t e^{-j2\pi n\Delta f\tau_t}$ (exact for slow-time shaped frames where $M^{-1}\sum_{m=0}^{M-1}r_{n,m} = 1$ almost surely, and a conditional-mean benchmark for i.i.d. baselines). By the Slepian-Bangs formula (exact for dense Rayleigh multipath $K_c \gg 1$ by the CLT),

$$\begin{aligned}J(\tau_t) &= \frac{2M}{\sigma_{\text{int}}^2(q_t)}\sum_{n=-N/2}^{N/2-1}|\partial_{\tau_t}\mu_n(\tau_t)|^2\\ &= \frac{2MNP_tB_{\text{rms}}^2}{\sigma_{\text{int}}^2(q_t)} = \text{CRLB}(\hat{\tau}_t)^{-1},\end{aligned}$$

proving (14). ∎

Appendix D
Proof of Theorem 2

For Part (a), $\mathbf{s} \sim \mathcal{U}(\sqrt{M}\,\mathbb{S}^{2M-1})$ has $\mathbf{s} \overset{d}{=} \sqrt{M}\,\mathbf{g}/\|\mathbf{g}\|_2$ with $\mathbf{g} \sim \mathcal{CN}(\mathbf{0}, \mathbf{I}_M)$ and $u_m = |g_m|^2 \sim \text{Exp}(1)$. By the Gamma-Dirichlet relation, $\tilde{\mathbf{r}} = M^{-1}\mathbf{r} \sim \text{Dir}(\mathbf{1}_M)$ has

$$\mathbb{E}[\tilde{r}_m^2] = \frac{2}{M(M+1)}, \quad \mathbb{E}[\tilde{r}_m\tilde{r}_\ell] = \frac{1}{M(M+1)} \ \ (m \neq \ell).$$

Scaling by M^2 gives

$$\kappa_{\text{marg}}(M) = M^2\mathbb{E}[\tilde{r}_m^2] = \frac{2M}{M+1}, \qquad \text{Var}(r_m) = \frac{M-1}{M+1},$$

and $\text{Cov}(r_m, r_\ell) = -\frac{1}{M+1}$, proving (16).

For Part (b), let $\mathbf{u} \sim M\,\text{Dir}(\mathbf{1}_M)$ with $\mathbb{E}[\mathbf{u}] = \mathbf{1}_M$ and $\text{Cov}(\mathbf{u}) = \frac{M}{M+1}(\mathbf{I}_M - \frac{1}{M}\mathbf{1}_M\mathbf{1}_M^T)$. Since $\mathbf{1}_M \in \mathcal{V}_{\text{null}}$, $\mathbf{P}_\perp\mathbf{1}_M = \mathbf{0}$ and $\boldsymbol{\delta} \triangleq \mathbf{P}_\perp(\mathbf{u} - \mathbf{1}_M)$ has

$$\text{Cov}(\boldsymbol{\delta}) = \mathbf{P}_\perp\text{Cov}(\mathbf{u})\mathbf{P}_\perp = \frac{M}{M+1}\mathbf{P}_\perp.$$

Because $\mathcal{V}_{\text{null}}$ is spanned by shift-invariant Fourier harmonics (8), $\mathbf{P}_\perp$ is circulant with $[\mathbf{P}_\perp]_{m,m} = \frac{1}{M}\text{Tr}(\mathbf{P}_\perp) = \frac{M-d_{\text{null}}}{M}$, giving $\text{Var}(\delta_m) = \frac{M-d_{\text{null}}}{M+1}$ and

$$\kappa_{\text{proj}}(M, d_{\text{null}}) = 1 + \text{Var}(\delta_m) = \frac{2M + 1 - d_{\text{null}}}{M+1}$$

in (17). Under radial retraction $\mathbf{r} = \mathbf{1}_M + \alpha(\mathbf{u})\boldsymbol{\delta} \in \mathcal{P}_M(\mathcal{Q}_{\text{null}})$,

$$\mathbf{V}_{\text{null}}^T(\mathbf{r} - \mathbf{1}_M) = \alpha(\mathbf{u})\mathbf{V}_{\text{null}}^T\mathbf{P}_\perp(\mathbf{u} - \mathbf{1}_M) = \mathbf{0}$$

almost surely, preserving $\mathcal{V}_{\text{null}} \subset \ker(\mathbf{C}_{\text{slow}})$ and exact nulling in Theorem 1(a), with

$$\begin{aligned}\kappa_{\text{ret}}(M, d_{\text{null}}) &= 1 + \frac{1}{M}\mathbb{E}\big[\alpha(\mathbf{u})^2\|\boldsymbol{\delta}\|_2^2\big] \\ &= 1 + \bar{\alpha}_2^2\frac{M - d_{\text{null}}}{M+1} \le \kappa_{\text{proj}}(M, d_{\text{null}}).\end{aligned}$$

This completes the proof. ∎

Appendix E
Proofs of Theorem 3 and Proposition 3

For Theorem 3(a), under $\mathbf{Y} = \sqrt{\rho}\,\mathbf{S} + \mathbf{Z}$ ($\mathbf{Z} \sim \mathcal{CN}(\mathbf{0}, \mathbf{I}_L)$), rotational invariance of $\mathbf{S}$ implies rotational invariance of $\mathbf{Y}$, so $h(\mathbf{Y})$ decomposes in hyperspherical coordinates into $\log_2|\mathbb{S}^{2L-1}|$ plus the 1D radial entropy of $R^2 = \|\mathbf{Y}\|_2^2$ relative to $y^{L-1}\mathrm{d}y$. Since $h(\mathbf{Y}|\mathbf{S}) = L\log_2(\pi e)$ and $\mathbb{E}[R_{\text{sph}}^2] = \mathbb{E}[R_{\text{G}}^2] = L(1+\rho)$,

$$\begin{aligned}L\,\Delta I_{\text{sphere}}(L, \rho) &= \int_0^\infty f_{R_{\text{sph}}^2}(y)\log_2\frac{f_{R_{\text{sph}}^2}(y)}{f_{R_{\text{G}}^2}(y)}\,\mathrm{d}y \\ &= D_{\text{KL}}\Big(f_{R_{\text{sph}}^2}\,\Big\|\,f_{R_{\text{G}}^2}\Big),\end{aligned}$$

proving (18).

For Theorem 3(b), because $\mathbf{1}_M/\sqrt{M}$ is the first column of $\mathbf{V}_{\text{null}}$, every $\mathbf{r} \in \mathcal{P}_M(\mathcal{Q}_{\text{null}})$ satisfies $\|\mathbf{S}\|_2^2 = M$ almost surely, so $R^2 = \|\mathbf{Y}\|_2^2 \sim f_{R_{\text{sph}}^2}$ and the radial DPI $\mathbf{Y} \mapsto \|\mathbf{Y}\|_2^2$ gives $\Delta I_{\text{trench}}(M, d_{\text{null}}, \rho) \ge \Delta I_{\text{sphere}}(M, \rho)$. Splitting the M symbols into d_{null} disjoint sub-spheres $\mathcal{I}_1, \ldots, \mathcal{I}_{d_{\text{null}}}$ of lengths L_j with independent inputs $\mathbf{S}_{\mathcal{I}_j} \sim \mathcal{U}(\sqrt{L_j}\,\mathbb{S}^{2L_j-1})$ enforces d_{null} orthogonal energy constraints $\sum_{m\in\mathcal{I}_j} r_m = L_j$ and gives

$$I(\mathbf{S}_{\text{part}}; \mathbf{Y}) = \sum_{j=1}^{d_{\text{null}}} I(\mathbf{S}_{\mathcal{I}_j}; \mathbf{Y}_{\mathcal{I}_j}),$$

proving (19).

For Theorem 3(c), the DPI on $\mathbf{w}(\mathbf{Y}) \triangleq M^{-1/2}\mathbf{V}_{\text{null}}^T(|\mathbf{Y}|^{\odot 2} - (1+\rho)\mathbf{1}_M) \in \mathbb{R}^{d_{\text{null}}}$ gives $M\Delta I_{\text{trench}}(M, d_{\text{null}}, \rho) \ge D_{\text{KL}}(P_{\mathbf{w}(\mathbf{Y})}\|P_{\mathbf{w}(\mathbf{Y}_{\text{G}})})$. For $\mathbf{Y}_{\text{G}} \sim \mathcal{CN}(\mathbf{0}, (1+\rho)\mathbf{I}_M)$, $|Y_{\text{G},m}|^2 - (1+\rho)$ are i.i.d. sub-exponential with variance $(1+\rho)^2$, and $|[\mathbf{V}_{\text{null}}]_{m,i}| \le \sqrt{2/M}$ with $\mathbf{V}_{\text{null}}^T\mathbf{V}_{\text{null}} = \mathbf{I}_{d_{\text{null}}}$, so the multivariate CLT gives $\mathbf{w}(\mathbf{Y}_{\text{G}}) \xrightarrow{d} \mathcal{N}(\mathbf{0}, (1+\rho)^2\mathbf{I}_{d_{\text{null}}})$ as $M \to \infty$. Under clutter-trench shaping, $\mathbf{V}_{\text{null}}^T(\mathbf{r} - \mathbf{1}_M) = \mathbf{0}$ cancels the signal-intensity term in $|Y_m|^2 - (1+\rho) = \rho(r_m - 1) + 2\sqrt{\rho}\,\text{Re}(S_m^* Z_m) + (|Z_m|^2 - 1)$. Conditioned on $\mathbf{S}$, the remaining terms have conditional variance $1 + 2\rho + 4\rho(r_m - 1)$, so

$$\begin{aligned}\text{Cov}(\mathbf{w}(\mathbf{Y})|\mathbf{S}) &= (1+2\rho)\mathbf{I}_{d_{\text{null}}} \\ &\quad + \frac{4\rho}{M}\mathbf{V}_{\text{null}}^T\text{Diag}(\mathbf{r} - \mathbf{1}_M)\mathbf{V}_{\text{null}} \\ &\xrightarrow{p} (1+2\rho)\mathbf{I}_{d_{\text{null}}},\end{aligned}$$

and $\mathbf{w}(\mathbf{Y}) \xrightarrow{d} \mathcal{N}(\mathbf{0}, (1+2\rho)\mathbf{I}_{d_{\text{null}}})$. Evaluating the Gaussian KL divergence

$$\begin{aligned}&D_{\text{KL}}\big(\mathcal{N}(\mathbf{0}, (1+2\rho)\mathbf{I}_{d_{\text{null}}})\,\big\|\,\mathcal{N}(\mathbf{0}, (1+\rho)^2\mathbf{I}_{d_{\text{null}}})\big) \\ &\quad = \frac{d_{\text{null}}}{2\ln 2}\left[\ln\frac{(1+\rho)^2}{1+2\rho} - \frac{\rho^2}{(1+\rho)^2}\right]\end{aligned}$$

(with $\mathcal{O}(d_{\text{null}}^2/M^2)$ Edgeworth remainder) and dividing by M yields (20), matching the large-L_j expansion of (19). Equating the normal-approximation rates [22, Thm. 54]

$$\begin{aligned}C_{\text{AWGN}} - \sqrt{\frac{V_{\text{G}}}{N_{\text{blk}}L}}\,Q^{-1}(\epsilon) &= C_{\text{AWGN}} - \Delta I_{\text{sphere}} \\ &\quad - \sqrt{\frac{V_{\text{shell}}}{N_{\text{blk}}L}}\,Q^{-1}(\epsilon)\end{aligned}$$

gives (21).

For Proposition 3, at $L = 8$ with $(n_1, n_2, n_3) = (2, 4, 2)$, $\frac{8!}{2!\,4!\,2!} = 420 > 2^8$ gives $k_{\text{amp}} = 8$ and $2(2) + 4(3) + 2(4) = 24$ phase bits ($32/8 = 4.0000$ bits/symbol); at $L = 7$ with $(2, 3, 2)$, $\frac{7!}{2!\,3!\,2!} = 210 > 2^7$ gives $k_{\text{amp}} = 7$ and 21 phase bits ($28/7 = 4.0000$ bits/symbol). Squared radii $(r_{\text{ring},1}, r_{\text{ring},2}, r_{\text{ring},3}) = (0.32, 0.92, 1.84)$ for $L = 8$ give energy $8 = L$ and $\kappa_{\text{marg}} = \frac{10.3616}{8} = 1.2952$; squared radii $(0.31, 0.90, 1.84)$ for $L = 7$ give energy $7 = L$ and $\kappa_{\text{marg}} = \frac{9.3932}{7} = 1.3419$. Distinct ring permutations differ in at least two positions, with inter-ring squared distance $\min\{2(a_2 - a_1)^2, 2(a_3 - a_2)^2\} = 0.3097$ ($L = 8$) and 0.3071 ($L = 7$), and intra-ring squared distances $4a_1^2\sin^2(\pi/4) \ge 0.6200$ (QPSK), $4a_2^2\sin^2(\pi/8) \ge 0.5272$ (8-PSK), and

$$4a_3^2\sin^2(\pi/16) = 1.84\,d_{\text{min,16-PSK}}^2 = 0.2801 < 0.3071$$

on the outer 16-PSK ring (+2.65 dB). ∎

References

[1] F. Liu, Y. Cui, C. Masouros, J. Xu, T. X. Han, Y. C. Eldar, and S. Buzzi, "Integrated sensing and communications: Toward dual-functional wireless networks for 6G and beyond," *IEEE J. Sel. Areas Commun.*, vol. 40, no. 6, pp. 1728–1767, Jun. 2022, doi: 10.1109/JSAC.2022.3156632.

[2] C. Sturm and W. Wiesbeck, "Waveform design and signal processing aspects for fusion of wireless communications and radar sensing," *Proc. IEEE*, vol. 99, no. 7, pp. 1236–1259, Jul. 2011, doi: 10.1109/JPROC.2011.2131110.

[3] Y. Xiong, F. Liu, Y. Cui, W. Yuan, T. X. Han, and G. Caire, "On the fundamental tradeoff of integrated sensing and communications under Gaussian channels," *IEEE Trans. Inf. Theory*, vol. 69, no. 9, pp. 5723–5751, Sep. 2023, doi: 10.1109/TIT.2023.3284449.

[4] P. M. Woodward, *Probability and Information Theory, with Applications to Radar*. London, U.K.: Pergamon Press, 1953.

[5] F. Liu, Y. Xiong, S. Lu, S. Li, W. Yuan, C. Masouros, S. Jin, and G. Caire, "Uncovering the iceberg in the sea: Fundamentals of pulse shaping and modulation design for random ISAC signals," *IEEE Trans. Signal Process.*, vol. 73, pp. 2511–2526, 2025, doi: 10.1109/TSP.2025.3580596.

[6] F. Liu, Y. Zhang, Y. Xiong, S. Li, W. Yuan, F. Gao, S. Jin, and G. Caire, "CP-OFDM achieves the lowest average ranging sidelobe under QAM/PSK constellations," *IEEE Trans. Inf. Theory*, vol. 71, no. 9, pp. 6950–6967, Sep. 2025, doi: 10.1109/TIT.2025.3591267.

[7] Z. Liao, F. Liu, S. Li, Y. Xiong, W. Yuan, C. Masouros, and M. Lops, "Pulse shaping for random ISAC signals: The ambiguity function between symbols matters," *IEEE Trans. Wireless Commun.*, vol. 24, no. 4, pp. 2832–2846, Apr. 2025, doi: 10.1109/TWC.2024.3525440.

[8] Y. Zhang, F. Liu, Y. Xiong, W. Yuan, S. Li, L. Zheng, T. X. Han, C. Masouros, and S. Jin, "On discrete ambiguity functions of random communication waveforms," *arXiv:2512.08352*, 2025, doi: 10.48550/arXiv.2512.08352.

[9] Y. Ni, F. Liu, H. Yin, Y. Tang, Y. Ma, and Z. Wang, "Ambiguity function analysis of AFDM under pulse-shaped random ISAC signaling," *IEEE Trans. Wireless Commun.*, vol. 25, pp. 13619–13635, 2026, doi: 10.1109/TWC.2026.3670065.

[10] P. Zeng, Y. Lu, J. Tang, X. Chen, Y. Xiong, F. Liu, and S. Jin, "Statistical analysis of 3D ambiguity functions for random MIMO-OFDM signals," *arXiv:2610.12162*, 2026, doi: 10.48550/arXiv.2610.12162.

[11] C. E. Shannon, "Probability of error for optimal codes in a Gaussian channel," *Bell Syst. Tech. J.*, vol. 38, no. 3, pp. 611–656, May 1959, doi: 10.1002/j.1538-7305.1959.tb03905.x.

[12] G. Böcherer, F. Steiner, and P. Schulte, "Bandwidth efficient and rate-matched low-density parity-check coded modulation," *IEEE Trans. Commun.*, vol. 63, no. 12, pp. 4651–4665, Dec. 2015, doi: 10.1109/TCOMM.2015.2494016.

[13] P. Schulte and G. Böcherer, "Constant composition distribution matching," *IEEE Trans. Inf. Theory*, vol. 62, no. 1, pp. 430–434, Jan. 2016, doi: 10.1109/TIT.2015.2499181.

[14] Y. C. Gültekin, W. J. van Houtum, A. G. C. Koppelaar, and F. M. J. Willems, "Enumerative sphere shaping for wireless communications with short packets," *IEEE Trans. Wireless Commun.*, vol. 19, no. 2, pp. 1098–1112, Feb. 2020, doi: 10.1109/TWC.2019.2951139.

[15] Y. C. Gültekin, T. Fehenberger, A. Alvarado, and F. M. J. Willems, "Probabilistic shaping for finite blocklengths: Distribution matching and sphere shaping," *Entropy*, vol. 22, no. 5, Art. no. 581, May 2020, doi: 10.3390/e22050581.

[16] Z. Du, F. Liu, Y. Xiong, T. X. Han, Y. C. Eldar, and S. Jin, "Reshaping the ISAC tradeoff under OFDM signaling: A probabilistic constellation shaping approach," *IEEE Trans. Signal Process.*, vol. 72, pp. 4782–4797, 2024, doi: 10.1109/TSP.2024.3465499.

[17] Y. Zhang, S. Aditya, and B. Clerckx, "Input distribution optimization in OFDM dual-function radar-communication systems," *IEEE Trans. Signal Process.*, vol. 72, pp. 5258–5273, 2024, doi: 10.1109/TSP.2024.3491899.

[18] S. Lu, F. Liu, F. Dong, Y. Xiong, J. Xu, Y.-F. Liu, and S. Jin, "Random ISAC signals deserve dedicated precoding," *IEEE Trans. Signal Process.*, vol. 72, pp. 3453–3469, 2024, doi: 10.1109/TSP.2024.3427373.

[19] R. Laroia, N. Farvardin, and S. A. Tretter, "On optimal shaping of multidimensional constellations," *IEEE Trans. Inf. Theory*, vol. 40, no. 4, pp. 1044–1056, Jul. 1994, doi: 10.1109/18.335969.

[20] G. D. Forney, Jr., "Trellis shaping," *IEEE Trans. Inf. Theory*, vol. 38, no. 2, pp. 281–300, Mar. 1992, doi: 10.1109/18.119687.

[21] A. R. Calderbank and L. H. Ozarow, "Nonequiprobable signaling on the Gaussian channel," *IEEE Trans. Inf. Theory*, vol. 36, no. 4, pp. 726–740, Jul. 1990, doi: 10.1109/18.53734.

[22] Y. Polyanskiy, H. V. Poor, and S. Verdú, "Channel coding rate in the finite blocklength regime," *IEEE Trans. Inf. Theory*, vol. 56, no. 5, pp. 2307–2359, May 2010, doi: 10.1109/TIT.2010.2043769.

[23] A. Bemani, N. Ksairi, and M. Kountouris, "Affine frequency division multiplexing for next generation wireless communications," *IEEE Trans. Wireless Commun.*, vol. 22, no. 11, pp. 8214–8229, Nov. 2023, doi: 10.1109/TWC.2023.3260906.

[24] A. Bemani, N. Ksairi, and M. Kountouris, "Integrated sensing and communications with affine frequency division multiplexing," *IEEE Wireless Commun. Lett.*, vol. 13, no. 5, pp. 1255–1259, May 2024, doi: 10.1109/LWC.2024.3367178.

[25] R. Hadani, S. Rakib, M. Tsatsanis, A. Monk, A. J. Goldsmith, A. F. Molisch, and R. Calderbank, "Orthogonal time frequency space modulation," in *Proc. IEEE Wireless Commun. Netw. Conf. (WCNC)*, Mar. 2017, pp. 1–6, doi: 10.1109/WCNC.2017.7925924.

[26] L. Gaudio, M. Kobayashi, G. Caire, and G. Colavolpe, "On the effectiveness of OTFS for joint radar parameter estimation and communication," *IEEE Trans. Wireless Commun.*, vol. 19, no. 9, pp. 5951–5965, Sep. 2020, doi: 10.1109/TWC.2020.2998583.

[27] P. Kumari, J. Choi, N. González-Prelcic, and R. W. Heath, "IEEE 802.11ad-based radar: An approach to joint vehicular communication-radar system," *IEEE Trans. Veh. Technol.*, vol. 67, no. 4, pp. 3012–3027, Apr. 2018, doi: 10.1109/TVT.2017.2774762.

[28] C. D. Ozkaptan, H. Zhu, E. Ekici, and O. Altintas, "Software-defined MIMO OFDM joint radar-communication platform with fully digital mmWave architecture," in *Proc. IEEE Int. Symp. Joint Commun. Sens. (JC&S)*, Mar. 2023, pp. 1–6, doi: 10.1109/JCS57290.2023.10107511.

[29] J. Li, F. Tong, W. Jiang, and F. Zhang, "Metastructure-enabled underwater acoustic integrated sensing and communication," *IEEE Wireless Commun. Lett.*, vol. 13, no. 12, pp. 3335–3339, Dec. 2024, doi: 10.1109/LWC.2024.3462150.

[30] H. Özçörekci, G. N. Salduz, O. Gönen, E. Erdoğan, and İ. Altunbaş, "Low-cost integrated sensing and communication system design with ultrasonic sound waves," in *Proc. IEEE Signal Process. Commun. Appl. Conf. (SIU)*, 2026, pp. 1–4, doi: 10.1109/SIU71813.2026.11637043.